
















# Biocompatible Iron Oxide Nanoparticles Display Antiviral Activity Against Two Different Respiratory Viruses in Mice

Marta L DeDiego <sup>1,\*</sup>, Yadileiny Portilla <sup>2,\*</sup>, Neus Daviu <sup>2</sup>, Darío López-García <sup>1</sup>, Laura Villamayor <sup>1</sup>, Paula Vázquez-Utrilla <sup>1</sup>, Vladimir Mulens-Arias <sup>2</sup>, Sonia Pérez-Yagüe <sup>2</sup>, Aitor Nogales <sup>3</sup>, Jesús G Ovejero <sup>4</sup>, Alvaro Gallo-Cordova <sup>4</sup>, Luis Enjuanes <sup>1</sup>, Sabino Veintemillas-Verdaguer <sup>4</sup>, M Puerto Morales <sup>4</sup>, Domingo F Barber <sup>2</sup>

<sup>1</sup>Department of Molecular and Cellular Biology, Centro Nacional de Biotecnología (CNB-CSIC), Madrid, Spain; <sup>2</sup>Department of Immunology, Oncology and Nanobiomedicine Initiative, Centro Nacional de Biotecnología (CNB-CSIC), Madrid, Spain; <sup>3</sup>Center for Animal Health Research, CISA-INIA-CSIC, Madrid, Spain; <sup>4</sup>Department of Nanoscience and Nanotechnology, Instituto de Ciencia de Materiales de Madrid (ICMM-CSIC), Madrid, Spain

\*These authors contributed equally to this work

Correspondence: Domingo F Barber; Marta L DeDiego, Email [dfbarber@cnb.csic.es](mailto:dfbarber@cnb.csic.es); [marta.lopez@cnb.csic.es](mailto:marta.lopez@cnb.csic.es)

**Background:** Severe Acute Respiratory syndrome coronavirus 2 (SARS-CoV-2) and Influenza A viruses (IAVs) are among the most important causes of viral respiratory tract infections, causing similar symptoms. IAV and SARS-CoV-2 infections can provoke mild symptoms like fever, cough, sore throat, loss of taste or smell, or they may cause more severe consequences leading to pneumonia, acute respiratory distress syndrome or even death. While treatments for IAV and SARS-CoV-2 infection are available, IAV antivirals often target viral proteins facilitating the emergence of drug-resistant viral variants. Hence, universal treatments against coronaviruses and IAVs are hard to obtain due to genus differences (in the case of coronavirus) or subtypes (in the case of IAV), highlighting the need for novel antiviral therapies. Interestingly, iron oxide nanoparticles (IONPs) with a 10 nm core size and coated with the biocompatible dimercaptosuccinic acid (DMSA: DMSA-IONP-10) display antiviral activity against SARS-CoV-2 in vitro.

**Methods:** We analyzed the antiviral activity of DMSA-IONP-10 against SARS-CoV-2 infection in vivo, and against IAV infection in vitro and in vivo.

**Results:** DMSA-IONP-10 treatment of mice after SARS-CoV-2 infection impaired virus replication in the lungs and led to a mildly reduced pro-inflammatory cytokine induction after infection, indicating that these IONPs can serve as COVID-19 therapeutic agents. These IONPs also had a prophylactic and therapeutic effect against IAV in tissue cultured cells at non-cytotoxic doses, and a therapeutic effect in IAV-infected-mice, inhibiting viral replication and slightly dampening the inflammatory response after viral infection. As an exacerbated inflammatory response to IAVs and SARS-CoV-2 is detrimental to the host, weakening this response in mice through IONP treatment may reduce disease severity. Interestingly, our data suggest that IONP treatment affects oxidative stress and iron metabolism in cells, which may influence IAV production.

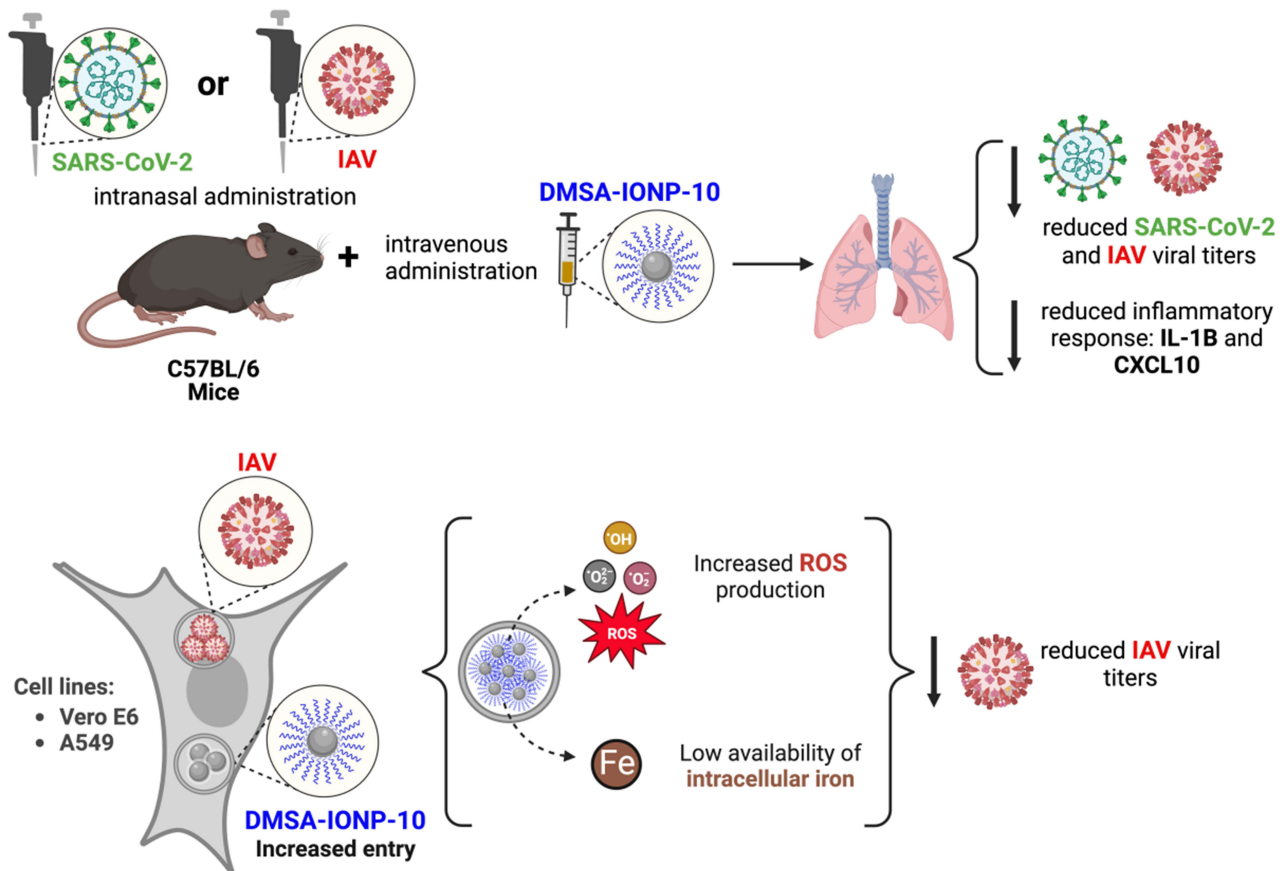
**Conclusion:** This study highlights the antiviral activity of DMSA-IONP-10 against important human respiratory viruses.

**Keywords:** iron oxide nanoparticles, SARS-CoV-2, IAV, viral infection, oxidative stress, iron metabolism

## Introduction

Severe Acute Respiratory syndrome coronavirus 2 (SARS-CoV-2) belongs to the *Coronaviridae* family, and it is an enveloped virus with a positive-sense, single-stranded RNA (ssRNA) genome of around 30 kb that can infect humans and other mammals. SARS-CoV-2 infection has spread globally, ultimately provoking the coronavirus pandemic that caused over 776 million confirmed cases up to October 2024 and over 7 million deaths globally, although these numbers are most likely underestimated.<sup>1</sup> Influenza viruses (IVs) belong to the *Orthomyxoviridae* family and they are also

## Graphical Abstract



enveloped viruses but with a segmented, negative-sense, ssRNA genome. IVs are divided into types A, B, C and D, with the type A (IAV) and B (IBV) producing global epidemics in humans each year.<sup>2</sup> Vaccination programs are implemented to combat IV infections but nevertheless, the World Health Organization (WHO) considers there are 1 billion infections every year, 3–5 million severe cases and around 500,000 deaths due to these viral infections. IAVs can be further subdivided into subtypes based on their viral surface glycoproteins hemagglutinin (HA, H1-H18) and neuraminidase (NA, N1-N11), H1N1 and H3N2 being the subtypes seasonally circulating in humans nowadays. However, sporadic human infection by different subtypes of avian viruses have become increasingly more common since 1997, raising the threat of a possibly devastating pandemic if any of these viruses evolve and become efficiently transmitted among humans.<sup>3–5</sup>

Current options available to treat COVID-19 include a range of antiviral agents or immune modifiers. However, novel antiviral agents or treatment strategies will be necessary to better reduce the ongoing morbidity and mortality caused by SARS-CoV-2. Remdesivir and Molnupiravir are among the best studied antiviral agents, which act by disrupting RNA transcription and viral replication, respectively.<sup>6,7</sup> Similarly Paxlovid™, which combines Nirmatrelvir (a SARS-CoV-2 3C-like main protease (Mpro) inhibitor that inhibits the growth of the virus) and Ritonavir (a boosting agent, that enhances Nirmatrelvir's performance), represents a promising treatment to significantly reduce hospitalization and the death of non-hospitalized patients who are at high risk of progressing to a severe illness.<sup>8</sup> Other current COVID-19 treatments include monoclonal antibodies (mAbs) targeting SARS-CoV-2.<sup>9</sup> However, the large-scale production of mAbs is extremely time consuming, labor-intensive and costly,<sup>10</sup> and the emergence of antigenically distinct viral strains diminishes their efficacy.<sup>6</sup>

Several antiviral agents have been approved to combat IV infections, although most target viral proteins and therefore, their use may lead to the selection of influenza strains resistant to these drugs. For example, amantadine<sup>11</sup> and rimantadine<sup>12</sup> are effective antiviral agents that target viral M2 proton channel activity but as IAV strains resistant to these drugs have been reported,<sup>11,12</sup> these drugs are no longer recommended for IAV treatment. NA inhibitors are currently available, such as zanamivir, oseltamivir, peramivir and laninamivir,<sup>13</sup> and while it is generally more difficult for IV strains to become resistant to NA inhibitors than to amantadine, it is still possible.<sup>13,14</sup> Thus, there remains a need to improve and synthesize new drugs to control IAV infections.

Due to the constant need to produce new strategies to combat SARS-CoV-2 and IAV infection, the possible antiviral activity of nanoparticles (NPs) is now being explored. The antiviral activity of metal and metal oxide NPs has been studied in relation to multiple viruses.<sup>15–18</sup> The selection of viral strains resistant to these agents appears to be negligible, and they could have also a broad spectrum against different viruses and opportunist pathogens that become virulent in unhealthy individuals. In this sense, we previously showed that iron oxide NPs (IONPs) and iron oxyhydroxide NPs (IOHNPs) impair the replication and transcription of SARS-CoV-2, as well as the production of infectious viruses by cells in culture. These effects were evident when these cells were treated either before or after infection, and it is an effect that is probably due to changes in oxidative stress and iron metabolism induced by the treatment with the NPs.<sup>19</sup>

Plaque inhibition assays and quantitative real-time PCR (RT-qPCR) of viral transcripts in the presence of glycine-coated IONPs suggested these have antiviral activity against IAV. Moreover, this activity appeared to involve the reaction of iron oxide with -SH groups of proteins in the cell, inactivating these proteins.<sup>20</sup> In addition, IONPs can catalyze lipid peroxidation of the viral lipid envelope due to their ability to induce the production of reactive oxygen species (ROS), thereby dampening the infectivity of the H1N1, H5N1 and H7N9 IAV subtypes.<sup>21</sup>

Silver NPs (Ag-NPs) can interact with IAVs, efficiently preventing their infection of cultured cells<sup>22</sup> and of mice,<sup>23</sup> diminishing any lung pathology and enhancing the survival of mice after infection. Furthermore, Ag-NP/chitosan composites with different NP sizes are active against H1N1 IAV, as witnessed by the reduced viral titers in viral suspensions after treatment with Ag-NP/Ch, and with smaller Ag-NPs displaying stronger antiviral activity against IAV.<sup>24</sup> In addition, the antiviral activity of Ag-NPs coated with influenza NA inhibitors like oseltamivir (Ag-NP-OTV)<sup>25</sup> and zanamivir (Ag-NP-ZNV)<sup>26</sup> has been analyzed, showing that the treatment of cells with the Ag-NPs, Ag-NP-OTV and Ag-NP-ZNV after the IAV infection reduces viral titers, being this effect higher for the Ag-NP-OTV and Ag-NP-ZNV than for Ag-NPs, and that, as expected, the Ag-NP-OTV and Ag-NP-ZNV affect the IAV NA activity, likely affecting the attachment of the virus to the host cells.<sup>25,26</sup>

Selenium NPs (Se-NPs) also display antiviral activity against IAVs, with data indicating that their antiviral activity can be further potentiated by coating them with the NA inhibitors zanamivir<sup>27</sup> or oseltamivir,<sup>28</sup> with the M2 inhibitor amantadine,<sup>29</sup> or with the influenza polymerase inhibitor ribavirin.<sup>30</sup> Moreover, the activity of Se-NPs against IAVs can be enhanced by coating the Se-NPs with b-thujaplicin (TP), an antimicrobial pentatrieneone (Se-NPs-TP).<sup>31</sup> Interestingly, the treatment of mice with Se-NPs-TP after IV infection prevents the lung pathology induced by infection and viral replication, and consequently enhances the survival of these mice.<sup>31</sup>

Among the different IONPs we tested for antiviral activity against SARS-CoV-2 in tissue culture cells in our study mentioned above, we found that magnetic IONPs produced by thermal decomposition in organic medium, with a core diameter of 10 nm and coated with DMSA (DMSA-IONP-10), were the IONPs with the strongest antiviral activity.<sup>19</sup>

Several years ago, our group studied the toxicity and biotransformation of DMSA-IONP-10 in mice over three months. The results of these studies showed that after five retro-orbital intravenous (i.v.) injections, DMSA-IONP-10 nanoparticles accumulated in spleen, liver and lung tissues where they undergo a process of biodegradation, and although some signs of very mild toxicity were observed post-administration, these were transient and did not compromise mouse survival and health status 3 months after administration, supporting the use of DMSA-IONP-10 in biomedical applications.<sup>32</sup> Therefore, because the excellent antiviral activity in vitro of DMSA-IONP-10 and their biocompatibility in mice, we decided to test in vivo the antiviral activity of DMSA-IONP-10.

Here, DMSA-IONP-10 were shown to efficiently impair the production of infectious SARS-CoV-2 in mice, as well as IAV in cultured cells or mice, suggesting that these NPs may serve to combat SARS-CoV-2 and IAV infections. Furthermore, our results show that treating infectious viruses with DMSA-IONP-10 reduces viral infectivity, and that

treating cells with these IONPs affects their oxidative stress and iron metabolism, which probably accounts for their antiviral activity.

## Materials and Methods

### Materials

Iron(III) acetylacetonate 99% ( $\text{Fe}(\text{acac})_3$ ) and benzyl ether 99% (BE) were purchased from Acros Organics (Geel, Belgium); oleic acid 80% GPR Rectapur<sup>®</sup> (OA) and acetone (anhydrous) were purchased from VWR (Leicestershire); 1,2-dodecanediol 90% (ODA), ethanol (99.5% - ACS reagent), dimercaptosuccinic acid (DMSA, ~98%), dimethyl sulfoxide (DMSO,  $\geq 99.7\%$ ) and potassium ferricyanide 0.8% were obtained from Sigma Aldrich (San Luis, MO, USA); oleylamine (OAM) 70% technical grade, was obtained from Merck; toluene 99.5% EssentQ<sup>®</sup> was purchased from Scharlau (Madrid); Dulbecco's modified Eagle's medium (DMEM) was purchased from Gibco (Invitrogen, CA); Fetal Bovine Serum (FBS) was obtained from Fisher; Mouse Serum (MS) was obtained from Sigma-Aldrich; PrestoBlue reagent was obtained from ThermoFisher Scientific; the anti-Nucleoprotein antibody was purchased from ATCC (HB-65: H16-L10-4R5); the total RNA extraction kit was purchased from Omega Bio-tek (GA, USA); the High-Capacity cDNA Reverse-Transcription kit, SYBR Green PCR Master and TaqMan gene expression assays were obtained from Applied Biosystems; the High Pure RNA Isolation Kit was purchased from Roche; C57BL/6 male mice were purchased from Envigo; agarose was obtained from Pronadisa; RNAlater was purchased from Ambion; glutaraldehyde, osmium tetroxide and epoxy resin TAAB 812 were obtained from TAAB Laboratories; DHR probe was purchased from Molecular probes, (Carlsbad, CA, USA).

### Synthesis and Physicochemical Characterization of IONPs

Magnetic iron oxide cores of 10 nm in diameter were prepared by thermal decomposition of  $\text{Fe}(\text{acac})_3$  in BE, in the presence of OA, OAM and ODA, according to reference.<sup>33</sup> In brief, the mixture containing the iron precursor (0.1 M), OA, OAM and ODA (molar ratio of  $\text{Fe}(\text{acac})_3$ :OA:OAM:ODA= 1:3:3:2) was stirred mechanically at 100 rpm with nitrogen for 1.5 h. The reactor was then heated up to 200°C at 3°C/min, left for two hours and then heated again to 286°C at 9°C/min. The product was then washed three times with a mixture of toluene (99.5%) and ethanol (1:2 v/v), sonicated for 15 min and separated magnetically.

Particles were transferred to water by ligand exchange using DMSA to displace OA and OAM. The IONPs were first precipitated from the hydrophobic suspension (50 mg) by adding ethanol, centrifuging and removing the solution, and the precipitate was then dispersed in 20 mL of toluene and mixed with 5 mL of DMSO containing DMSA (100 mg). The mixture was kept in a rotary shaker for 24 h and after discarding the supernatant, the IONPs coated with DMSA were washed several times with ethanol. Finally, the IONPs were redispersed in alkaline water, dialyzed and filtered through a 0.2  $\mu\text{m}$  membrane, thereafter referred to as DMSA-IONP-10.

The IONP particle size was determined by Transmission Electron Microscopy (TEM), with the iron oxide phase analyzed by X-ray diffraction (Bruker D8 Advance with Cu  $K\alpha$  radiation: data not shown) and the colloidal stability (ie hydrodynamic size and surface charge) studied by dynamic light scattering (DLS: Zetasizer, Malvern Instrument). Elemental analyses were performed by inductively coupled plasma optical emission spectroscopy after aqua regia digestion (ICP-OES: Perkin Elmer-2400) and the magnetic properties of the NPs using a SQUID magnetometer at room temperature and 5 K (Quantum Design MPMS-5), with a maximum magnetic field  $\pm 5$  T. The NPs were lyophilized and then, packed in a gelatin capsule to measure the hysteresis loop, normalizing the magnetization values as a function of the Fe concentration calculated by ICP-OES. The amount and composition of the coating was determined by Fourier Transform Infrared Spectroscopy (FTIR) in a Bruker IFS 66 V-S spectrometer and a Nicolet FT-IR 20SXC. Finally, a thermogravimetric (TG) analysis was performed on a Seiko TG/DTA 320U device.

### Cell Cultures

The African Green monkey kidney-derived epithelial Vero E6 cells were obtained from ATCC (CRL-1586), Vero cells expressing the TMPRSS2 protease (Vero-TMPRSS2) were obtained from Japanese Collection of Research Bioresources



(JCRB) Cell Bank in Japan (JCRBno. JCRB1819), Madin-Darby canine kidney (MDCK) cells were obtained from ATCC (CCL-34), and human lung adenocarcinoma A549 cells were obtained from ATCC (CCL-185). All cell lines were all grown in DMEM supplemented with 25 mM HEPES, 10% FBS and 100 U/mL streptomycin.

## Analysis of IONP Cytotoxicity

*PrestoBlue assay.* A549 cells were seeded in 96-well plates at a density of  $3 \times 10^4$  cells per well in a final volume of 100  $\mu$ L. After a 24 h incubation at 37°C, the A549 cells were treated with different concentrations of DMSA-IONP-10 (0–500  $\mu$ g Fe/mL) for an additional 24 h. The PrestoBlue reagent was then added to each well for 2 h in the same culture conditions and the fluorescence was measured (560 nm excitation; 590 nm emission). The PrestoBlue reagent contains a blue, cell-permeable, non-fluorescent solution of resazurin that can be metabolized inside cells to a red and fluorescent compound called resorufin, a shift that serves as an indicator of cell viability. Cell viability is indicated by the number of fluorescent treated cells relative to the fluorescent untreated cells.

## Quantification of Intracellular Iron After IONP Treatment

Vero E6 and A549 cells were seeded in a 6-well plate ( $1 \times 10^5$  cells per well) and cultured for 24 h at 37°C. The cells were then incubated for 3, 6 or 24 h with DMSA-IONP-10 (50 or 250  $\mu$ g Fe/mL). Alternatively, the Vero E6 cells in 6-well plates were infected with IAV (multiplicity of infection – MOI 1) and 1 h post-infection (hpi), the cells were treated for 24 h with the highest concentration of DMSA-IONP-10. Subsequently, the cells were washed three times with phosphate buffer saline (PBS) to remove the non-internalized NPs, they were harvested and then counted in a Neubauer chamber. The samples were digested with 1 mL of HNO<sub>3</sub> for 1 h at 90°C and the amount of iron per cell was measured by ICP-OES.

## Antiviral Activity of IONPs in Tissue Cultured Cells

The prophylactic effect of DMSA-IONP-10 was assessed by treating confluent monolayers of Vero E6 and A549 cells (in 24-well plates) with these particles at 50 or 250  $\mu$ g Fe/mL for 24 h. The cells were then infected with IAV (A/PuertoRico/8/1934 strain or PR8 strain) for 24 and 48 h at a MOI 1, collecting the cell culture media at 24 and 48 hpi for titration. Besides, to assess the prophylactic effect of IONPs on virus replication and transcription, the same experiment was performed but the cells were collected at 6 and 16 hpi to purify their total RNA for gene expression analysis.

To analyze the therapeutic effect of DMSA-IONP-10, confluent monolayers of Vero E6 and A549 cells (24-well plates) were infected with IAV (MOI 1), and the IONPs were added to the media at 1 hpi at the same concentrations as those used to study the prophylactic effect. The medium was collected at 24 and 48 hpi, and titrated, and total RNA to assess therapeutic effect on virus replication and transcription was purified from cells collected at 6 and 16 hpi. IAV virus titrations were performed in MDCK cells grown in 96-well plates and infected over 14 h with 10-fold serial dilutions of the virus at 33°C. An immunofocus assay (focus-forming units [FFU]/mL) was then performed using the HB-65 anti-Nucleoprotein antibody.

## The Effect of IONPs on Virus Replication and Transcription

To analyze whether the therapeutic and prophylactic treatment of cells with DMSA-IONP-10 influences viral replication and/or transcription directly, total RNA from untreated and DMSA-IONP-10-treated Vero E6 cells, either mock-infected or IAV-infected was collected at 6 and 16 hpi, as explained above. Total RNA was extracted using a total RNA extraction kit, according to the manufacturer's protocol. RT-qPCR was performed following an adapted protocol<sup>34</sup> in which purified RNA (1  $\mu$ g) was reverse-transcribed to cDNA using a High-Capacity cDNA Reverse-Transcription kit and the NPvRNA-5'-GGCCGTCATGGTGGCGAATGAATGGACGAAAAACAAGAATTGC-3' or NPmRNA-5'-CCAGATCGTTTCGAGTCGTTTTTTTTTTTTTTTTCTTTAATTGTC-3' primers, complementary to the viral RNA (vRNA) NP segment and the viral NP gene mRNA, respectively. RT-qPCR was then performed using the SYBR Green PCR Master mix and the Fw-NPvRNA 5'-CTCAATATGAGTGCAGACCGTGCT-3' and Rv-NPvRNA-5'-GGCCGTCATGGTGGCGAAT-3' primers, complementary to the NP vRNA segment and the Fw-NPmRNA-5'-

CGATCGTGCCTTCCTTTG-3' and Rv-NPmRNA-5'-CCAGATCGTTCGAGTCGT3' primers, complementary to the NP gene mRNA. The transcripts amplified were quantified using the threshold cycle ( $2^{-\Delta\Delta CT}$ ) method.<sup>35</sup>

## Analysis of DMSA-IONP-10 Treatment on Viral Infectivity

Cell culture supernatants containing  $10^5$  FFU IAV, were treated for 2 h at 37°C with medium containing DMSA-IONP-10 at 250 or 50 µg Fe/mL, or with medium alone. The infectious virus titers were then evaluated through an immunofocus assay in MDCK cells, as indicated above.

## The Antiviral Effect of DMSA-IONP-10 in SARS-CoV-2 and IAV-Infected Mice

C57BL/6 male mice, 12-weeks-old or 6-8-weeks-old, were purchased one week before inoculation with SARS-CoV-2 or IAV, respectively, and they were housed under pathogen-free conditions at the Animal Health Research Center (INIA-CISA, Madrid, Spain), or at the animal facilities of the National Center for Biotechnology (Centro Nacional de Biotecnología – Consejo Superior de Investigaciones Científicas – CNB-CSIC, Madrid, Spain). All the protocols involving mice were approved by the CSIC ethics committee for animal experimentation and by the Division of Animal Protection of the regional government of Madrid, and they followed National and European Union legislation on animal experimentation (PROEX125.7/21 for IAV infections and PROEX49.6/23 for SARS-CoV-2 infections). All mice involved in the *in vivo* experiments were given *ad libitum* access to the same diet throughout the study. Mice were mildly anesthetized with ketamine/xylazine and then, inoculated intranasally with 2000 FFU/mice of IAV (strain A/PuertoRico/8/1934) or with 5000 FFU/mice of a SARS-CoV-2 mouse-adapted strain described previously.<sup>36</sup> Subsequently, at 4 hours post-infection (hpi), and every 24 hours over the next three days, under mild isoflurane anesthesia, mice were retro-orbitally injected with DMSA-IONP-10 at a concentration of 0.16 mg Fe/mouse per injection, representing a total dose of 0.64 mg Fe/mouse after 4 injections, or with PBS as control (SARS-CoV-2 + IONPs, IAV + IONPs, SARS-CoV-2+ PBS, and IAV + PBS groups). Besides, for IAV and SARS-CoV-2 *in vivo* experiment, a group of mice was left uninfected and inoculated with PBS as control (N=4). A total of 6, 8, 10, and 9 mice per SARS-CoV-2 + IONPs, SARS-CoV-2+ PBS, IAV + IONPs, and IAV + PBS groups, respectively, were used for the *in vivo* experiments. The body weight of mice was evaluated throughout the *in vivo* experiments and the body weight loss was determined relative to the starting weight. Mice losing more than 25% of their initial body weight were considered to have reached the experimental end-point and were sacrificed humanely. At 4 days post-infection (dpi), all the mice were sacrificed and their lungs were extracted for analysis.

IAV and SARS-CoV-2 replication was evaluated by assessing the viral titers in the lungs at 4 dpi. As such, the right superior and middle lung lobules were extracted and homogenized, and IAV titers were determined in immunofocus assays on MDCK cells as indicated above. By contrast, the SARS-CoV-2 titers were determined in plaque titration assays on Vero-TMPRSS2 cells. To this end, Vero-TMPRSS2 cells were grown in 24-well plates and infected with 10-fold serial dilutions of the virus. After 1 h absorption, the cells were overlaid with low electroendosmosis agarose and incubated for 3 days at 37°C. The cells were then fixed with 10% formaldehyde in PBS and permeabilized with 20% methanol, and the viral plaques were visualized and counted using crystal violet, and expressed as plaque forming units (PFU) per mL of lung homogenate. In addition, total RNA was extracted from the right inferior and post-caval lobules, and the *Cxcl10*, *Il-1b*, *Sod2* and *Duox2* mRNA in the lungs were analyzed at 4 dpi. Hence, the left lung lobules were extracted and incubated in RNA later at 4°C for 24 h prior to adding the lungs to RNA lysis buffer and homogenizing them manually in a dounce homogenizer. Total RNA was extracted from the homogenized lungs using the total RNA kit. RT was then performed for 2 h at 37°C to generate cDNAs using the High-Capacity cDNA transcription kit and random hexamers. qPCR analysis using TaqMan gene expression assays specific for the murine *Cxcl10* (Mm00445235\_m1) and *Il-1b* (Mm00434228\_m1), and specific for the mouse *GAPDH* gene (Mm99999915\_g1) were then carried out. Alternatively, the cDNAs were then analyzed by qPCR with a Power SYBR Green PCR mix and primers specifically designed to amplify *Mus musculus* transcripts for the genes *Sod2* and *Duox2* (Table S1), synthesized by Sigma-Aldrich. The data were analyzed using the threshold cycle ( $2^{-\Delta\Delta CT}$ ) method<sup>35</sup> and normalized to the *GAPDH* expression.

## Analyses of the Presence of DMSA-IONP-10 in Lung Tissues

The presence of DMSA-IONP-10 in lung tissues was evaluated in TEM images. As such, approximately 1 mm<sup>3</sup> of lung tissue was fixed for 30 min at room temperature in 4% paraformaldehyde (PFA) and 2.5% glutaraldehyde diluted in PBS. The tissue was then transferred to fresh buffered fixative solution for 1 h at room temperature and then left overnight at 4°C. The tissue was then washed with PBS, post-fixed for 1 h at 4°C with 1% osmium tetroxide in potassium ferricyanide 0.8% and then maintained for 1 h in 2% aqueous uranyl acetate at 4°C. After washing with distilled water, the tissues were dehydrated with increasing concentrations of acetone, embedded in epoxy resin TAAB 812 and polymerized in epoxy resin (100%) over 2 days at 60°C. The resin blocks were then trimmed and ultrathin, 70 nm thick sections were obtained on an UC6 ultramicrotome (Leica Microsystems). The sections were transferred to 200 mesh nickel grids (Gilder) and stained at room temperature for 20 min with saturated aqueous uranyl acetate and for 1 min in lead citrate 0.2% (Electron Microscopy Sciences). The sections were visualized on a JEOL JEM 1400 Flash electron microscope (operating at 100 kV) and micrographs were obtained with a Gatan OneView digital camera at various magnifications.

In addition, the left lung lobule was extracted and used for ICP-OES analysis after nitric acid and aqua regia digestion, and for magnetic measurements with a SQUID magnetometer after lyophilization and packing in a gelatin capsule without cotton to avoid contamination. Hysteresis loops were recorded at room temperature and at 5 K, and the magnetic behavior of the NPs was used as a reference to quantify them in the lungs.

## Analysis of Oxidative Stress in Cells Treated with DMSA-IONP-10

### Dihydrorhodamine 123 (DHR) Staining

The production of ROS was quantified by dark-field confocal staining with the DHR probe, a non-fluorescent ROS indicator that can be oxidized inside cells to the fluorescent rhodamine 123. A549 cells were cultured on coverslips in 24-well plates for 24 h and the cells were then treated for 24 h with a DMSA-IONP-10 suspension (250 µg Fe/mL). As a positive control of oxidative stress, the A549 cells were incubated for 1 h with H<sub>2</sub>O<sub>2</sub> (1 mM). The coverslips were then washed with PBS and the cells incubated for 30 min with DHR (diluted 1:500 in medium) under cell culture conditions. After washing with PBS, the cells were fixed for 15 min with PFA (4%), stained for 10 min with DAPI (diluted 1:500 in PBS), washed and mounted with Fluoromount-G. Images were obtained under a dark-field Leica TCS SP5 confocal microscope with the 63X oil objective, using a 488 nm laser light for dark-field acquisition of the IONPs and quantifying the DHR signal intensity with Image J software.

### RT-qPCR Analysis of the Effect of the IONPs on the Expression of Genes Involved in the Antioxidant Response

A549 cells were treated for 24 h with a DMSA-IONP-10 suspension (250 µg Fe/mL), collected, and the total RNA from untreated and treated cells was extracted using the High Pure RNA Isolation Kit. The RNA was quantified with NanoDrop, and 2 µg of RNA was reverse-transcribed to cDNA using the High-Capacity cDNA Reverse Transcriptase kit and random primers. The cDNA was then analyzed by qPCR with a Power SYBR Green PCR mix and primers specifically designed to amplify *Homo sapiens* transcripts of the following genes (see [Table S1](#)): catalase (*CAT*); dual oxidases 1 and 2 (*DUOX1*, *DUOX2*); superoxide dismutase 1, 2 and 3 (*SOD1*, *SOD2*, *SOD3*); and thioredoxin reductase 2 (*TXNRD2*). The primers were synthesized by Sigma-Aldrich, and the RT-qPCR data was analyzed by the threshold cycle ( $2^{-\Delta\Delta CT}$ ) method<sup>35</sup> and normalized to *GAPDH* expression.

## The Effect of Oxidative Stress Induction on IAV Replication

Confluent monolayers of Vero E6 and A549 cells (24-well plates) were treated for 24 h with N-Acetyl-L-Cysteine (NAC, 200 µM), a recognized ROS scavenger,<sup>37</sup> or left untreated as a control. The cells were then infected with IAV (MOI 1) and the extracellular medium containing the virus was replaced at 1 hpi with a suspension of the DMSA-IONP-10 and NAC (200 µM), or with a suspension of the DMSA-IONP-10 without NAC as a control. After 48 h the medium was collected and the virus was titrated in an immunofocus assay, as described above.

## The Effect of DMSA-IONP-10 Treatment on Iron Metabolism Genes

To analyze the effect of IONPs on genes involved in iron metabolism, Vero E6 cells were treated for 24 h with a DMSA-IONP-10 suspension (250 µg Fe/mL), or these cells were infected with IAV and 1 hpi, they were treated with the same concentration of DMSA-IONP-10 for 24 h. The total RNA from both untreated and treated cells was extracted with the High Pure RNA Isolation Kit (Roche), quantified using NanoDrop, and 2 µg of RNA was reverse-transcribed to cDNA using the High-Capacity cDNA Reverse Transcriptase kit and random primers. The cDNA was used to perform RT-qPCR with a Power SYBR Green PCR mix and primers designed specifically to amplify transcripts for the: Transferrin Receptor (*TFRC*), *SLC11A2* (encoding divalent metal transporter 1, DMT1), *SLC48A1* (encoding heme transporter 1, HRG1), *SLC40A1* (encoding ferroportin, FPN1), iron responsive element binding protein 2 (*IREB2*) and lipocalin 2 (*LCN2*, encoding neutrophil gelatinase-associated lipocalin-NGAL) according to the *Chlorocebus sabaeus* predicted mRNA sequences (NCBI taxonomy number 60711, see [Table S2](#)).<sup>19</sup> The primers were synthesized by Sigma-Aldrich, and the RT-qPCR data was analyzed by the threshold cycle ( $2^{-\Delta\Delta CT}$ ) method<sup>35</sup> and normalized to *GAPDH* expression.

### Statistical Analysis

All the data are presented as the mean ± standard deviation (SD) and analyzed with a Student's *t*-test, one-way or two-way analysis of variance (ANOVA), applying a Tukey's and Dunnett's test to calculate the differences between the distinct values. Values of  $p < 0.05$  were considered statistically significant: \*  $p < 0.05$ , \*\*  $p < 0.01$ , \*\*\*  $p < 0.001$ , and \*\*\*\*  $p < 0.0001$ . GraphPad Prism version 9.5.1 was used for all the statistical analyses.

## Results

### DMSA-IONP-10 Production and Physicochemical Characterization

As mentioned in the introduction, in a previous study, our group evaluated the antiviral potential of various coated IONPs against SARS-CoV-2 infections in vitro. Among the different IONPs we tested, we found that magnetic IONPs produced by thermal decomposition in organic medium, with a core diameter of 10 nm and coated with DMSA (DMSA-IONP-10), were the IONPs with the strongest antiviral activity against SARS-CoV-2 in tissue culture cells.<sup>19</sup> Therefore, we wanted to evaluate the antiviral activity of DMSA-IONP-10 against SARS-CoV-2 in vivo in a mouse model of infection.

For this study a new batch of DMSA-IONP-10 was produced and the main physicochemical characteristic of this new batch was ascertained ([Figure 1](#)), confirming that this batch was indistinguishable from previous batches of DMSA-IONP-10 used in previous studies of the group<sup>19,32,38–41</sup> DMSA-IONP-10 have spherical shape ([Figure 1A](#)) with a size distribution of  $10 \pm 2$  nm ([Figure 1B](#)). The magnetization measurements confirmed the superparamagnetic behavior of the DMSA-IONP-10 at room temperature (RT, see [Figure 1C](#)). The characteristic infrared bands detected through Fourier-transform infrared spectroscopy (FTIR) demonstrated that the IONPs were coated with the corresponding organic compounds ([Figure 1D](#)), showing peaks at  $1625$  and  $1383$   $\text{cm}^{-1}$  for DMSA and Fe–O bond-specific IR bands between  $400$  and  $850$   $\text{cm}^{-1}$ . To quantify the amount of polymer bound to the iron oxide core of the DMSA-IONP-10, thermogravimetric (TG) analysis was performed. The mass percentage of the coatings was approximately 15% for the DMSA-IONP-10 ([Figure 1E](#)). Finally, the stability of DMSA-IONP-10 was assessed using dynamic light scattering (DLS) measurements after incubating the IONPs in water, PBS, or DMEM supplemented with 10% mouse serum (MS, DMEM-MS) for 0, 24, 48, 72 or 96 hours ([Figure 1F](#)). The results obtained show that the DMSA-IONP-10 have a similar hydrodynamic size in water ( $\sim 86.11 \pm 5.27$  nm) and PBS ( $\sim 124.78 \pm 16.62$  nm), and that this size remains constant over time, indicating that they are stable, even in PBS, which is the vehicle used for administration in the animal model. Regarding the hydrodynamic size of DMSA-IONP-10 incubated in DMEM-MS, a condition that simulates the environment in the bloodstream following intravenous administration in the in vivo model, we observed that the NPs increase in size ( $283.0 \pm 48.65$  nm) due to interactions with serum proteins and the formation of a protein corona, a process previously described by the group with similar NPs.<sup>32,38,42</sup> Nevertheless, it is important to note that their stability is not compromised, as only a single peak is observed in the size distribution, and their polydispersity indices indicate they remain monodisperse. These results are concomitant with those previously shown by our group,<sup>32</sup> and confirm that DMSA-IONP-10 are feasible for in vivo applications.

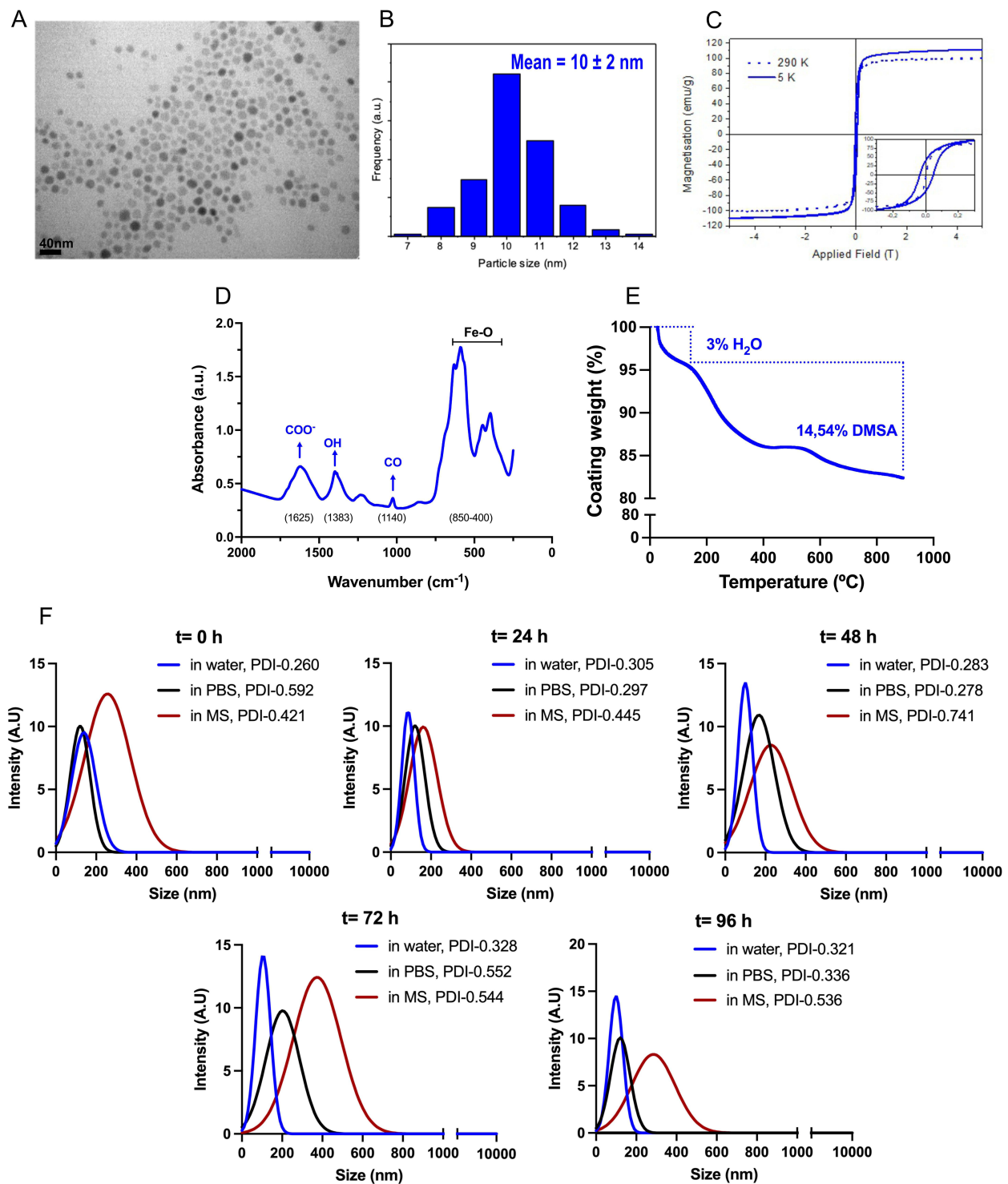


**Figure 1** Physicochemical characterization of DMSA-IONP-10.

**Notes:** (A) TEM images of spherical DMSA-IONP-10. Scale bar: 40 nm. (B) Distribution of the iron core diameter (nm) of at least 200 IONPs. (C) Magnetic properties of DMSA-IONP-10, showing superparamagnetic behavior at room temperature and ferromagnetic behavior at 5 K. (D) FTIR spectra of DMSA-IONP-10. Characteristic IR 1625, 1383 and 1140  $\text{cm}^{-1}$  bands were detected corresponding to  $\text{COO}^-$ , OH and CO groups. Iron-oxygen bands were detected at 850–400  $\text{cm}^{-1}$ . (E) Density of the DMSA coating determined by thermogravimetric (TG) analysis showing 17.54% DMSA coverage of the iron core surface. (F) Characterization of the stability of DMSA-IONP-10 over time (0, 24, 48, 72 and 96 h) determined by DLS. DMSA-IONP-10 were incubated during the mentioned hours in water, in PBS, and in DMEM with 10% MS. Polydispersity indices (PDI) are shown in all cases.



## DMSA-IONP-10 Accumulated in the Lung After i.v. Injection

In a previous study by our group, we had observed that after retro-orbital i.v. injections in mice of biocompatible DMSA-IONP-10, these nanoparticles were detected in the lungs and to a lesser extent in spleen and liver.<sup>38</sup> Following these observations, we conducted a study of the biodistribution, toxicity and degradation of DMSA-IONP-10 *in vivo*, which confirmed our previous observations and allowed us to characterize more precisely when the presence of nanoparticles begins to be detected in the different organs and the time it takes them to be degraded. In this study DMSA-IONP-10 NPs were detected in the lungs as early as 30 min after i.v. injection and they persisted for up to 90 days post-inoculation, although gradual degradation was evident over time, indicating that the IONPs are cleared from the body.<sup>32</sup> To confirm that the new DMSA-IONP-10 batch synthesized for this study reached the lungs in mice and to quantify the DMSA-IONP-10 that accumulated there, three different doses of DMSA-IONP-10 were i.v. injected retro-orbitally into C57BL/6 mice on consecutive days (4 days) to reach total doses of 0.48, 0.64 and 0.80 mg Fe per mouse after the four injections, with 0.80 mg Fe per mouse after the four injections being the maximum dose that can be administered in retro-orbital i.v. injections for four consecutive days. One day after the last dose was administered, the mice were sacrificed, their lungs were extracted and lyophilized, and the presence of IONPs was confirmed by magnetic measurements in a SQUID magnetometer ([Supplemental Figure S1A](#)). This technique detects the presence of IONPs in the tissue, quantifying them through the magnetic behavior of the IONPs as a function of the field. There were considerable differences in the magnetization curves between the lung tissue samples from control mice injected with PBS and lung tissue samples from mice injected with DMSA-IONP-10, when administered at doses of 0.48 mg Fe/mouse and 0.64 mg Fe/mouse, reflecting the accumulation of DMSA-IONP-10 in the lungs ([Supplemental Figure S1B](#)). A non-linear dependence of magnetization with the field (“S” shape) was evident, characteristic of ferromagnetic materials like magnetite with zero coercivity at room temperature (ie superparamagnetic behavior) and non-zero coercivity (350–400 Oe) at 5 K, similar to the IONP curves ([Figure 1C](#)). By contrast, magnetization has a linear dependence with the field at both temperatures for the PBS control samples, diamagnetic in most cases (negative) or paramagnetic (positive) when there is some residual blood in the lungs. Lung tissue samples from mice treated with the highest dose of 0.80 mg Fe/mouse were not measured in a SQUID magnetometer because at this dose, although all the mice remain alive and no obvious changes in the body weight of mice were observed during the treatments at any of the doses ([Supplemental Figure S1C](#)), some signs of toxicity (eye necrosis, piloerection) were observed, and therefore, we decided not to use this dose for the antiviral activity studies.

## SARS-CoV-2 Antiviral Effect of DMSA-IONP-10 in Mice

Having confirmed that the batch of DMSA-IONP-10 synthesized for this study could reach the lungs ([Supplemental Figure S1B](#)), we evaluated the antiviral activity of these nanoparticles against SARS-CoV-2 *in vivo* in a mouse model of infection. For these experiments, the dose of DMSA-IONP-10 that allows the highest nanoparticle concentration detected in the lungs without induction of toxicity in mice was used: a total dose of 0.64 mg Fe/mouse administered in 4 i.v. injections of 0.16 mg Fe/mouse for each individual injection. C57BL/6 mice were inoculated intranasally with 5000 PFU of a mouse-adapted strain of SARS-CoV-2, which reproduces many aspects of the disease seen in humans.<sup>36</sup> At 4 hpi and every 24 hours over the next three days, mice were intravenously inoculated with 0.16 mg Fe/injection of DMSA-IONP-10, reaching a total of 0.64 mg Fe/mouse after 4 injections (SARS-CoV-2 + IONPs group), or intravenously inoculated with PBS (SARS-CoV-2 + PBS group). The mice were then sacrificed at 4 dpi ([Figure 2A](#)) and the presence of IONPs in the lungs were evaluated by SQUID magnetometer to confirm the superparamagnetic behavior in DMSA-IONP-10 treated mice compared to PBS treated control mice ([Figure 2B](#)). By measuring the maximum magnetization in the lungs at 5K (0.004 emu/g – 0.0013 emu/g of organ) and comparing this with that for the IONPs (110 emu/g Fe), the NPs that reached the lungs was estimated to be between 0.036 mg Fe and 0.012 mg Fe per gram of organ. Taking into account an average weight of 0.2 grams per lung, this represents between the 1.13 and 0.34% of the injected dose. The weight loss evaluated over the 4 days of infection showed that infected mice lost weight as a consequence of infection ([Figure 2C](#)), as expected,<sup>36</sup> although all the mice remained alive during the 4-day-experiment. Interestingly, SARS-CoV-2-infected mice treated with the DMSA-IONP-10 lost slightly less weight than the untreated SARS-CoV-2-infected control mice

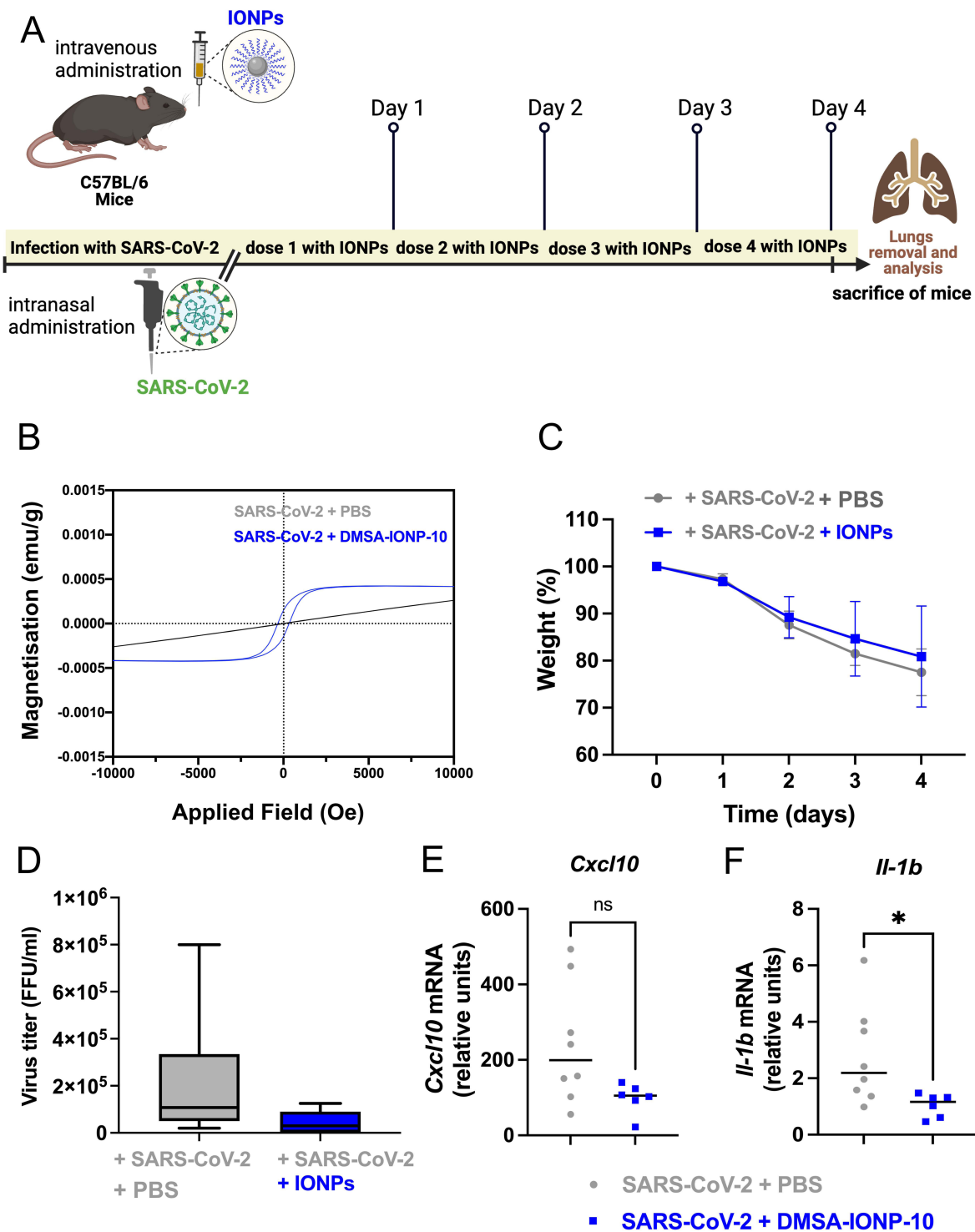


**Figure 2** SARS-CoV-2 antiviral effect of DMSA-IONP-10 in mice.

**Notes:** Groups of 12-week-old mice were inoculated intranasally with 5000 FFU/mouse. At 4 hpi, and over the next 3 days, mice were inoculated intravenously with DMSA-IONPs-10 (N = 6) or with PBS as a control (N = 8), and they were then sacrificed at 4 dpi. **(A)** Experimental timeline. **(B)** Presence of DMSA-IONP-10 in the lungs detected by SQUID magnetometer, showing ferromagnetic behavior at 5 K in the DMSA-IONP-10-treated mice compared to the paramagnetic behavior in the PBS control mice. The graph represents an example of one lung of the DMSA-IONP-10-treated mice versus one lung of the PBS treated mice after SARS-CoV-2 infection. **(C)** Body weights of SARS-CoV-2 infected mice were monitored over 4 days after receiving PBS (grey) or DMSA-IONP-10 (blue). **(D)** Viral titer evaluated by plaque analysis. **(E and F)** Inflammatory responses were evaluated by the expression of the proinflammatory cytokines *Cxcl10* **(E)** and *Il-1b* **(F)** by RT-qPCR at 4 dpi. Increased mRNA levels in SARS-CoV-2-infected DMSA-IONP-10-treated or untreated mice were expressed as the fold change relative to the mock-infected, non-treated, control mice. Each dot corresponds to one IAV-infected mouse and the data is analyzed with a *t*-test: \**p* < 0.05 and ns, no significant differences.

(Figure 2C), further suggesting, as observed in the non-infected mice (Supplemental Figure S1C), that the treatment of mice with DMSA-IONP-10 is not toxic to the animals. Finally, the viral titers in the lungs at 4 dpi were determined through a plaque lysis analysis in Vero-TMPRSS2 cells. In the infected mice, a 3-fold reduction was observed in the DMSA-IONP-10 inoculated mice relative to the control mice treated with the vehicle alone (Figure 2D), reflecting the antiviral activity of DMSA-IONP-10 in vivo.

A very strong inflammatory response is correlated with disease severity after SARS-CoV-2 infections in patients.<sup>43,44</sup> To further assess whether treating mice with the NPs could reduce the inflammation provoked by SARS-CoV-2 infection, dampening the SARS-CoV-2-induced pathology, the expression of the pro-inflammatory cytokines *Cxcl10* and *Il-1b* in the mouse lungs was assessed by RT-qPCR. Weaker *Cxcl10* expression was observed in infected mice treated with DMSA-IONP-10 relative to those infected mice administered with the vehicle alone (Figure 2E). Furthermore, while *Il-1b* expression was enhanced in the infected mice that received the vehicle, it did not increase when these mice were treated with the IONPs (Figure 2F), suggesting that the NPs might be beneficial to the infected hosts by reducing lung viral titers, and by leading to a decreased inflammatory response induced after SARS-CoV-2 infection.

### Analysis of DMSA-IONP-10 Uptake and Toxicity in A549 Cells

Given the antiviral activity of DMSA-IONPs-10 against SARS-CoV-2 in both infected cultured cells<sup>19</sup> and mice (this article), we investigate the potential antiviral activity of these NPs against IAV, another relevant respiratory virus. The potential antiviral effect of DMSA-IONP-10 against IAV was first assessed in infected cell lines. For these experiments, we first determined the working concentrations for DMSA-IONP-10 in the two model cell lines commonly used to study IAV infection, Vero E6 and A549 cells. The PrestoBlue assay was used to determine cell viability, assessing mitochondrial metabolism as an indirect measure of cell viability. The working concentration of DMSA-IONP-10 for Vero E6 cells was determined previously to be 250  $\mu\text{g Fe/mL}$ , with cell viability remaining above 95% at this concentration.<sup>19</sup> The working dose of DMSA-IONP-10 in human lung epithelial A549 cells was determined using a PrestoBlue assay after a 24 h treatment with different concentrations of DMSA-IONP-10. DMSA-IONP-10 did not induce strong cytotoxicity, as the viability was >80% at concentrations as high as 250  $\mu\text{g Fe/mL}$  (Figure 3A). Therefore, we chose to use a working concentration of 250  $\mu\text{g Fe/mL}$  for DMSA-IONP-10 for both cell lines,<sup>19</sup> as well as a second lower working concentration (50  $\mu\text{g Fe/mL}$ ) at which Vero E6 and A549 cell viability was nearly 100%, to assess whether these treatments have any dose-dependent effects.

To investigate DMSA-IONP-10 uptake by A549 cells, cells were incubated for 3, 6 or 24 h with the two concentrations of DMSA-IONP-10 (50 or 250  $\mu\text{g Fe/mL}$ ) and the IONPs internalized by the cells were assessed by ICP-OES, measuring the intracellular iron concentration of the cultured cells. The dose and time-dependent iron uptake of DMSA-IONP-10 by Vero E6 cells has been published previously<sup>19</sup> and the maximal iron uptake by A549 cells was observed

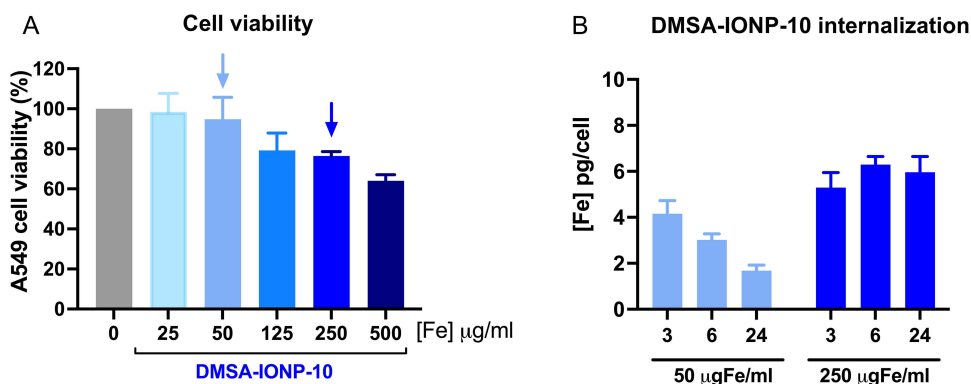


**Figure 3** Evaluation of DMSA-IONP-10 toxicity and iron uptake in A549 cells.

**Notes:** (A) Viability of A549 cells after a 24h treatment with different doses of DMSA-IONP-10, as measured with the PrestoBlue fluorometric test. (B) Iron uptake over time measured by ICP-OES after treating the cells with 50 and 250  $\mu\text{g Fe/mL}$  DMSA-IONP-10. The data represents the mean and SD from three independent experiments.

with the highest dose of DMSA-IONP-10 (250  $\mu\text{g Fe/mL}$ ) at 6 h (5.55 pg Fe/cell: [Figure 3B](#)). Thus, both cell lines internalized the DMSA-IONP-10.

## Effect of DMSA-IONPs-10 on Infectious Viral Production

To analyze the effect of DMSA-IONP-10 on IAV production, Vero E6 cells were treated with these particles for 24 h before infection (prophylactic effect) or for 1 h after infection (therapeutic effect), measuring the viral titers in the cell culture supernatants at 24 and 48 hpi ([Figure 4A](#)). The maximum DMSA-IONP-10 concentration had a prophylactic effect and reduced viral titers at 48 hpi by 98.8% ([Figure 4A](#)). In terms of the therapeutic effect, the highest, non-cytotoxic concentration of DMSA-IONP-10 reduced the viral titers at 48 hpi by 97% ([Figure 4A](#)). Therefore, therapeutic and prophylactic treatment of cells with DMSA-IONP-10 significantly diminished the production of infectious IAV viruses.

To confirm that the IAV antiviral effect of DMSA-IONP-10 also occurs in infected human cells, similar experiments were performed on A549 human lung adenocarcinoma cells ([Figure 4B](#)). The highest concentration of DMSA-IONP-10 had a prophylactic effect, reducing the viral titers in cell culture supernatants by 99.97% and 99.95% at 24 and 48 hpi, respectively ([Figure 4B](#)). In therapeutic terms, the highest DMSA-IONP-10 concentration reduced viral titers by 91% at 24 hpi ([Figure 4B](#)).

## The Effect of IONPs on Viral Replication and Transcription

To analyze whether the therapeutic and prophylactic treatment of cells with DMSA-IONP-10 influences viral replication and/or transcription directly, Vero E6 cells were exposed to DMSA-IONP-10 before or after IAV infection, and genomic RNA (vRNA) and NP mRNA expression was determined by RT-qPCR at 6 and 16 hpi to evaluate viral replication and transcription, respectively. After prophylactic exposure, the expression of vRNA and NP mRNA did not decrease in cells treated with DMSA-IONP-10 relative to the untreated control cells, except for the 2-fold reduction in NP mRNA at 16 hpi when the highest dose of DMSA-IONP-10 was administered ([Figure 5A](#)). The therapeutic treatment of cells with both doses of DMSA-IONP-10 after IAV infection only reduced the amounts of NP mRNA at 6 hpi, ([Figure 5B](#)), a reduction that did not persist at 16 hpi. These results strongly suggest that treating cells with DMSA-IONP-10 before or after the infection did not significantly affect viral replication or transcription.

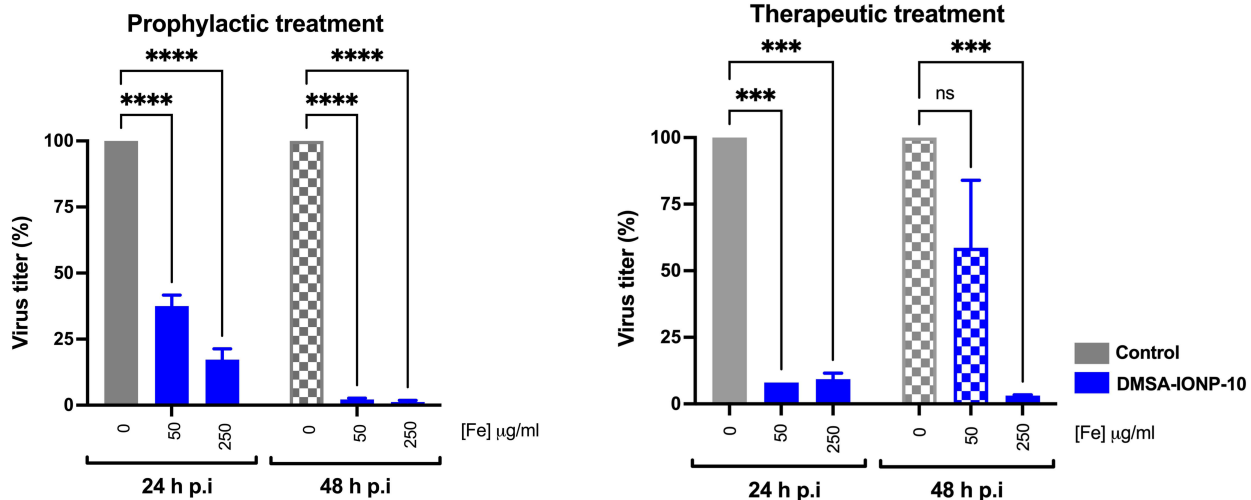
## The Effect of DMSA-IONP-10 Treatment on Virus Infectivity

Treatment of IAV with iron oxide nanozymes reduces viral infectivity by catalyzing lipid peroxidation of the viral envelope.<sup>21</sup> To analyze whether treating the viruses with DMSA-IONP-10 reduces their infectivity, cell culture supernatants containing viruses were exposed to medium containing DMSA-IONP-10 at 250 and 50  $\mu\text{g Fe/mL}$  for 2 h, or with medium alone, and the infectious virus titers were then evaluated. The treatment of viruses with the highest concentration of DMSA-IONP-10 reduced the viral titers 3-fold ([Figure 5C](#)), suggesting that DMSA-IONP-10 can directly dampen viral infectivity.

## In vivo Antiviral Effect of DMSA-IONP-10 Against IAV

Since promising results were observed with both the prophylactic and therapeutic treatment of cells in vitro, reducing the production of IAV infectious viruses, the antiviral activity of DMSA-IONP-10 was evaluated in vivo. C57BL/6 mice were inoculated intranasally with IAV (A/PuertoRico/8/1934 strain) at 2000 FFU/mouse and at 4 hpi, and on the following 3 days, mice were injected retro-orbitally with DMSA-IONP-10 (0.16 mg Fe/mice per injection, resulting in a total dose of 0.64 mg Fe/mouse after the 4 injections) (+IAV PR8 + IONPs group) or injected with PBS (+IAV PR8 + PBS group) ([Figure 6A](#)). These mice were sacrificed at 4 dpi, and the IONPs that reached the lungs in this setting was quantified by measuring the magnetic moment of the lungs at 5 K (between 0.0084 emu/g and 0.0022 emu/g) and compared to the magnetic behavior of the IONPs (110 emu/g Fe: [Figure 6B](#)). Between 0.075 mg Fe and 0.02 mg Fe was detected in the lungs per gram of organ ([Figure 6B](#)), representing between 2.2% and 0.6% of the injected dose (0.64 mg Fe), assuming an average weight of 0.2 grams per lung. In addition, the presence of DMSA-IONP-10 in the lungs was corroborated in TEM images, showing these IONPs to accumulate in the lung after infection and DMSA-IONP-10

## A Vero E6 cells



## B A549 cells

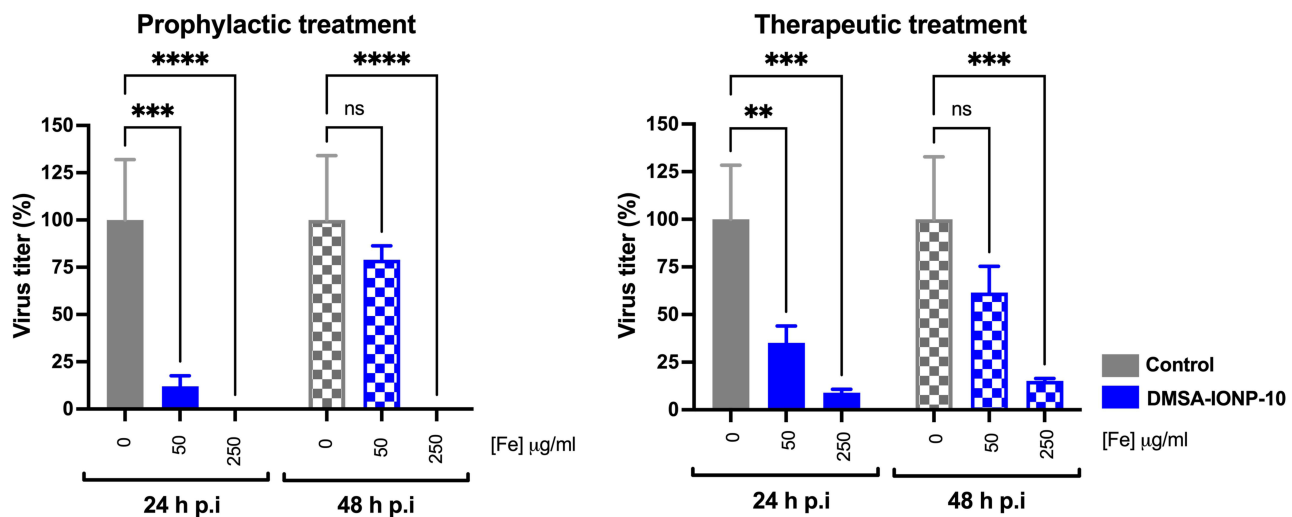


**Figure 4** Prophylactic and therapeutic antiviral effect of DMSA-IONP-10 in cells.

**Notes:** Vero E6 (A) or A549 (B) cells were treated with DMSA-IONP-10 at the two different concentrations indicated, or left untreated (control cells), and 24 h after treatment the cells were infected with IAV (prophylactic treatment). Alternatively, Vero E6 (A) or A549 (B) cells were infected with IAV and 1 hpi they were treated with DMSA-IONP-10 (therapeutic treatment). (A and B) Cell culture supernatants were collected at 24 and 48 hpi, and the viral titer was determined by an immunofocus assay in MDCK cells. Viral titers were assessed and represented relative to the titers in control, untreated cells (%). The data (mean  $\pm$  SD) are from three independent experiments and analyzed by two-way ANOVA followed by a Dunnett's multiple comparison test: \*\* $p < 0.01$ ; \*\*\* $p < 0.001$ ; and \*\*\*\* $p < 0.0001$ ; and ns, no significant differences.

treatment (Supplemental Figure S2). Significantly, the infected mice, either treated or not with DMSA-IONP-10, lost no significant weight during the 4 days of the experiment (Figure 6C), suggesting that in this animal model, neither IAV, nor the DMSA-IONP-10 treatment cause significant disease in the mice. Interestingly, the viral titers in the lungs at 4 dpi were 4-fold lower in the DMSA-IONP-10 inoculated mice than in the control mice treated with the vehicle alone (Figure 6D), reflecting the antiviral effects of the DMSA-IONP-10 in vivo.

An exacerbated inflammatory response has been correlated with disease severity after IAV infection in vivo.<sup>45,46</sup> Thus, to further assess whether treating mice with the NPs could reduce the inflammation induced after IAV infection, pro-inflammatory *Cxcl10* and *Il-1b* cytokine expression in the mouse lungs from infected animals treated with DMSA-IONP-10 or with vehicle alone, was measured by RT-qPCR, and compared to the expression in non-treated, non-infected mice. A mild decrease in *Cxcl10* and *Il-1b* expression was observed after infection in the mice treated with the NPs



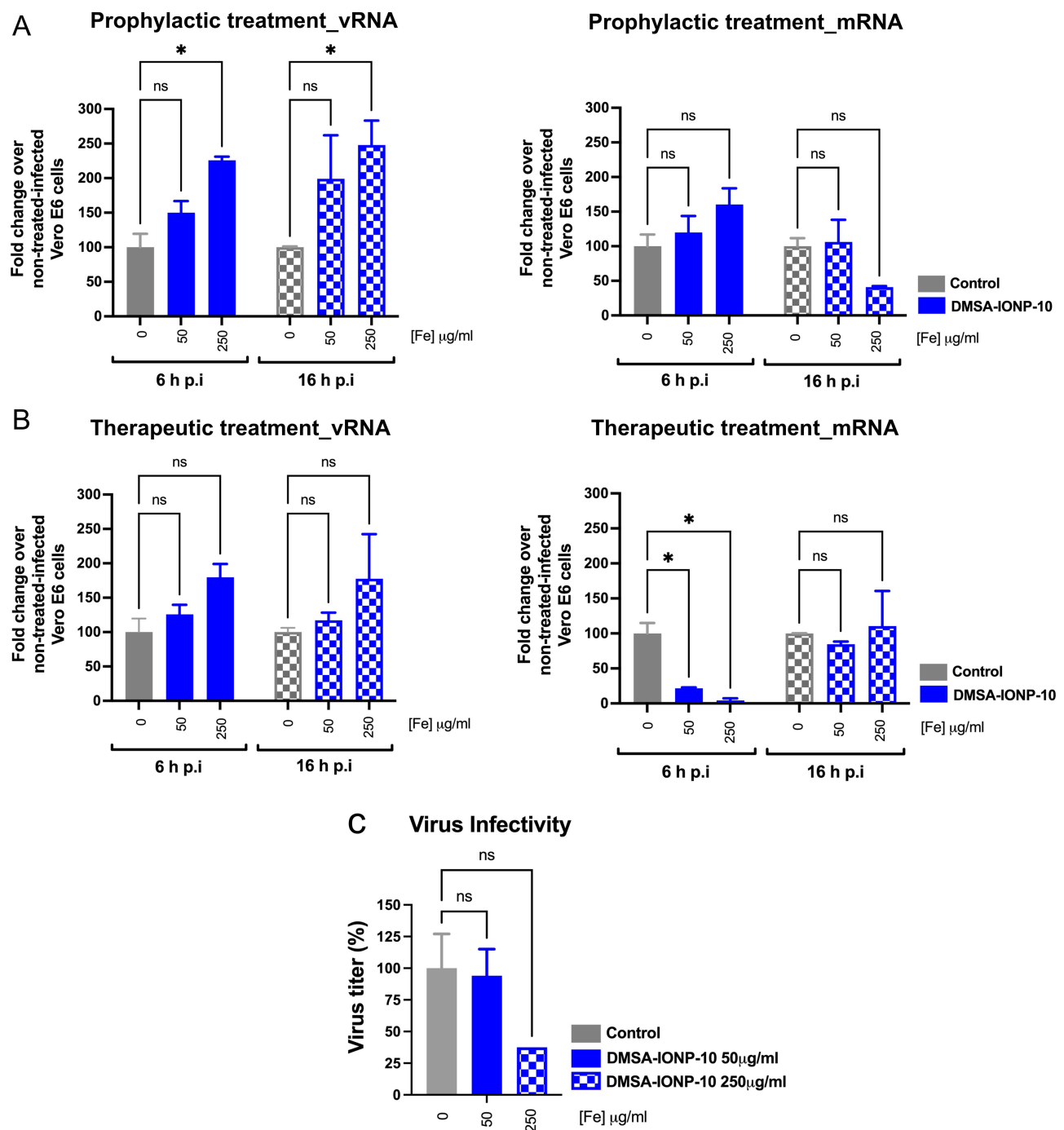


**Figure 5** Effect of DMSA-IONP-10 on viral replication, transcription and infectivity.

**Notes:** (A and B) Effect of treatment of cells with DMSA-IONP-10 before or after the infection on IAV replication and transcription. (A) Vero E6 cells were treated with DMSA-IONP-10 at two different concentrations, or left untreated (control cells), and 24 h after treatment the cells were infected with IAV (MOI 1) for an additional 6 or 16 h. (B) Vero E6 cells were infected with IAV and 1 hpi they cells were treated with DMSA-IONP-10 for 6 or 16 h as indicated in A. (A and B) Total RNA was extracted at 6 and 16 hpi, and the vRNA, NP mRNA and GAPDH RNA expressed was quantified by RT-qPCR. The vRNA and mRNA expression was normalized to that of GAPDH, and represented relative to the expression in control, untreated cells (%). (C) The effect of DMSA-IONP-10 treatment on virus infectivity. Infectious viruses were incubated with medium containing DMSA-IONP-10 at 50 and 250 µg Fe/mL for 2 h at 37°C, and virus infectivity was then evaluated in an immunofocus assay, determining the viral titers relative to those in the controls treated with medium alone (%). The data (mean ± SD) were representative of three independent experiments and they were evaluated by two-way ANOVA followed by a Dunnett's multiple comparison test: \*p < 0.05 and ns, no significant differences.

relative to those treated with PBS (Figure 6E and 6F). These data correlate with the lower virus titers observed in the mouse lungs from DMSA-IONP-10-treated mice, compared to the viral titers in vehicle-treated mice and suggest that NP treatment of mice might benefit the host by leading to a milder inflammation after IAV infection.

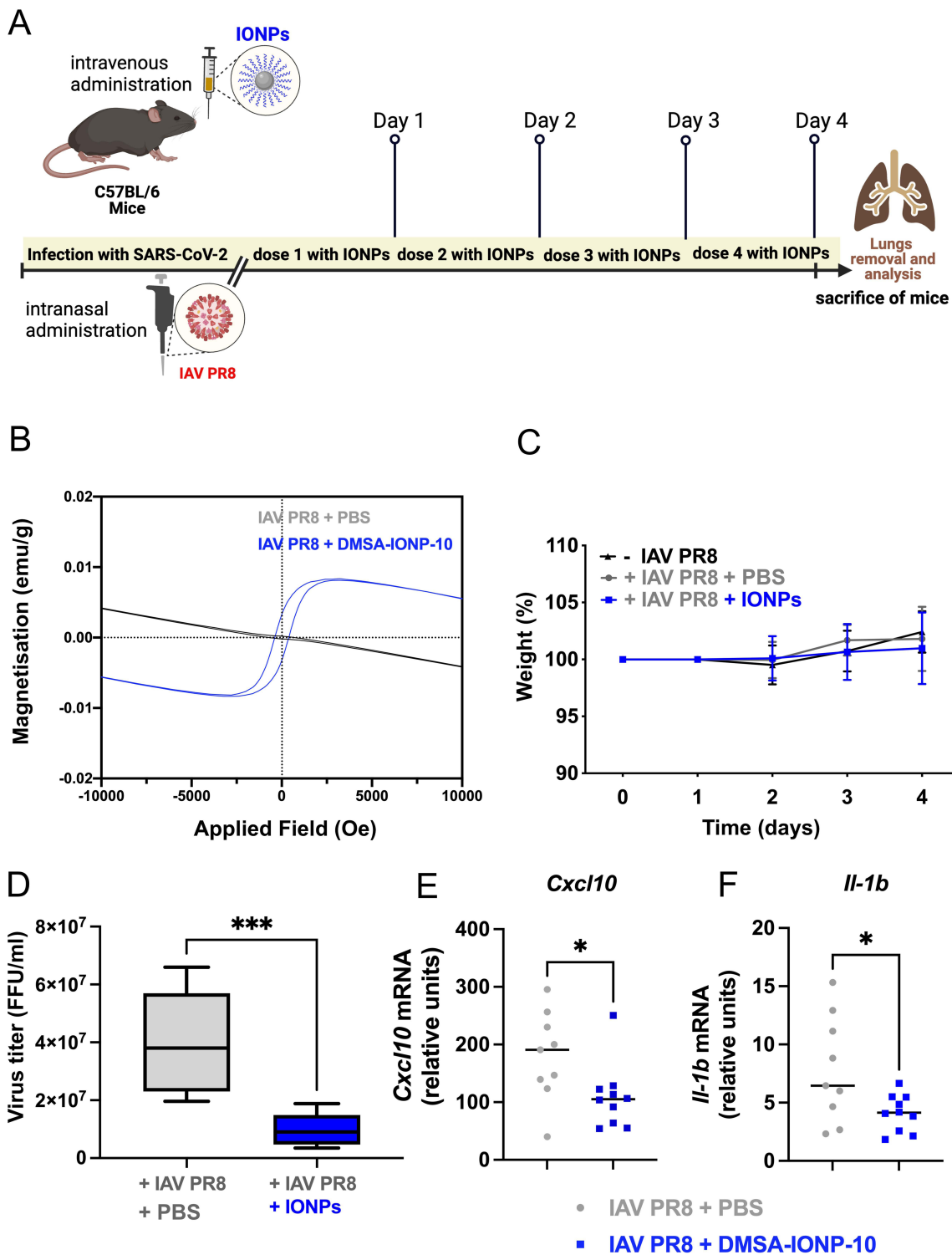


**Figure 6** Influenza antiviral effect of DMSA-IONP-10 in mice.

**Notes:** Groups of 6 to 8-week-old mice were inoculated intranasally with 2000 FFU/mice and at 4 hpi, and every day over the next 3 days, the mice were inoculated intravenously with DMSA-IONP-10 (N = 10) or with PBS as a control (N = 9), sacrificing them at 4 dpi. **(A)** Experiment timeline. **(B)** The levels of iron in mice were evaluated at 4 dpi by SQUID magnetometer at 5 K. The graph represents an example of one lung of the DMSA-IONP-10 treated mice versus one lung of the PBS treated mice after IAV infection. **(C)** The weight of the was assessed just before infection and daily from day 0 to day 4 after infection. **(D)** Viral titers in the DMSA-IONP-10 treated and control mouse lungs were measured with an immunofocus assay in MDCK cells at 4 dpi. **(E and F)** *Cxcl10* **(E)** and *Il-1b* **(F)** expression in the mouse lungs was evaluated by RT-qPCR at 4 dpi. Increases in mRNA in IAV-infected, DMSA-IONP-10 treated mice or untreated mice were expressed as the fold change relative to mock infected mice as controls. Each dot corresponds to one IAV-infected mouse and the data was analyzed with a t-test: \*p < 0.05 and \*\*\*p < 0.001.

## Induction of Oxidative Stress as a Consequence of DMSA-IONP-10 Cell Uptake and Its Effect on the IONP's Antiviral Activity

It is well known that one of the cytotoxic effects of IONPs is the production of ROS, which in turn triggers oxidative stress in cells. We previously showed that one of the possible antiviral mechanisms of IONPs against SARS-CoV-2 infection in Vero E6 cells was the induction of oxidative stress.<sup>19</sup> To determine whether oxidative stress induced by DMSA-IONP-10 could be partially responsible for their antiviral effect against IAV in infected cells, it is important to determine the capacity of these IONPs to induce ROS in these cells. ROS induction was studied in A549 cells, since we previously described that DMSA-IONP-10 induce ROS in Vero E6 cells (18). A549 cells were treated for 24 h with DMSA-IONP-10 (250 µg Fe/mL) and then, the cells were stained with the DHR probe that only fluoresces inside the cells when oxidized by ROS. DMSA-IONP-10-treated cells induced a 3.5-fold change in DHR fluorescence relative to the control A549 cells (1 a.u. of fluorescence) (Figure 7A), whereas in Vero E6 cells DMSA-IONP-10 produced a 10-fold change in DHR fluorescence relative to the control.<sup>19</sup>

The oxidative stress induced was further studied by assessing the antioxidant responses induced by DMSA-IONP-10 in A549 cells, quantifying the expression of antioxidant enzymes like catalase (Cat), superoxide dismutases (*SOD* 1, 2 and 3), dual oxidases (*DUOX* 1 and 2), and thioredoxin reductase 2 (*TXNRD2*), by RT-qPCR.<sup>47</sup> We previously showed that DMSA-IONP-10 induced the expression of *DUOX1*, *DUOX2*, *SOD1*, *SOD2*, *SOD3* and thioredoxin domain containing 2 (*TXNDC2*) antioxidant genes in Vero E6 cells<sup>19</sup> and here, we found that DMSA-IONP-10 induced the expression of *DUOX1*, *DUOX2*, *SOD2* and *SOD3* in A549 cells (Figure 7B). Hence, DMSA-IONP-10 appear to induce significant oxidative stress in Vero E6 and A549 cells, activating different antioxidant machineries (Figure 7A and 7B).

Whether the oxidative stress induced by DMSA-IONP-10 contributes to their IAV antiviral activity was analyzed in Vero E6 cells, in which these IONPs induced more intense oxidative stress. Cells were infected with IAV and then treated with DMSA-IONP-10 at 1 hpi, with or without the ROS scavenger NAC,<sup>37</sup> as it was previously shown that NAC treatment of IONP loaded cells inhibits ROS production by DHR analysis (Supplemental Figure S3). The highest dose of DMSA-IONP-10 induced ROS production by the cells, although the ROS produced by DMSA-IONP-10 administered together with NAC was similar to that observed in the control cells, indicating that NAC does indeed dampen the ROS produced by DMSA-IONP-10 treatment. Interestingly, the viral titers at 48 hpi were similar in Vero E6 control cells irrespective of whether they were treated with NAC or not (Figure 7C). However, in cells exposed to DMSA-IONP-10, viral titers increased when the cells were also exposed to NAC relative to those in cells that remained untreated in the original medium (Figure 7C). Importantly, the treatment of Vero E6 cells with NAC does not significantly affect IONP internalization, indicating that the effect of NAC on viral titers is not due to an altered internalization of the IONPs.<sup>19</sup> These results suggested that ROS production by DMSA-IONP-10-treated cells was at least partially responsible for the antiviral effect of these IONPs.

In order to analyze whether the increase of oxidative stress induced by DMSA-IONPs-10 is detectable at the organ level in mice, RNA was extracted from lungs from IAV or SARS-CoV-2-infected mice, treated with DMSA-IONPs-10 or with PBS, at 4 dpi. The mRNA expression of some oxidative stress response genes was analyzed by RT-qPCR. For this analysis, we chose to analyze the expression of *Duox2* and *Sod2*, because they were the oxidative stress response genes that were most strongly induced after the treatment of A549 cells with DMSA-IONP-10 (Figure 7B). This analysis using total RNA extracted from lungs, showed a tendency to express higher levels of *Sod2* and *Duox2* mRNAs in lungs from SARS-CoV-2-infected, DMSA-IONP-10-treated mice, than in lungs from SARS-CoV-2-infected, PBS-treated mice. However, this difference was not statistically significant for the *Duox2* gene, and this difference between DMSA-IONP-10-treated mice and PBS-treated mice was not observed among the IAV-infected mice (Supplemental Figure S4).

## Changes in Iron Uptake and in the Expression of Transcripts Associated with Iron Metabolism as a Consequence of DMSA-IONP-10 Internalization by IAV-Infected Cells

To determine whether IAV infection alters iron uptake or metabolism, the intracellular iron content of mock-infected cells or Vero E6 cells infected and treated with DMSA-IONP-10 at the highest concentration at 1 hpi, was assessed (Figure 8A). The intracellular iron content measured by ICP-OES was slightly lower in mock-infected control cells

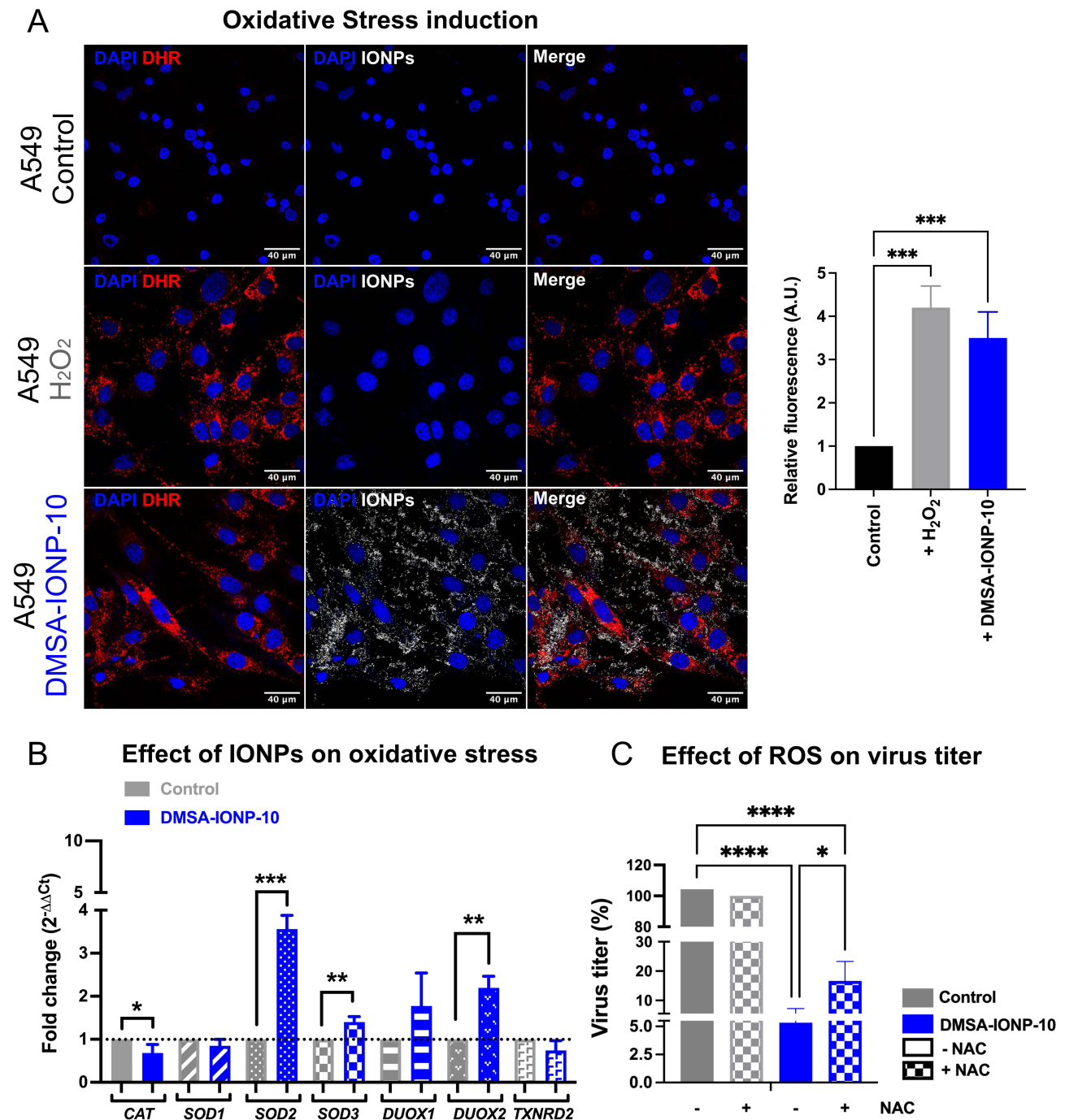


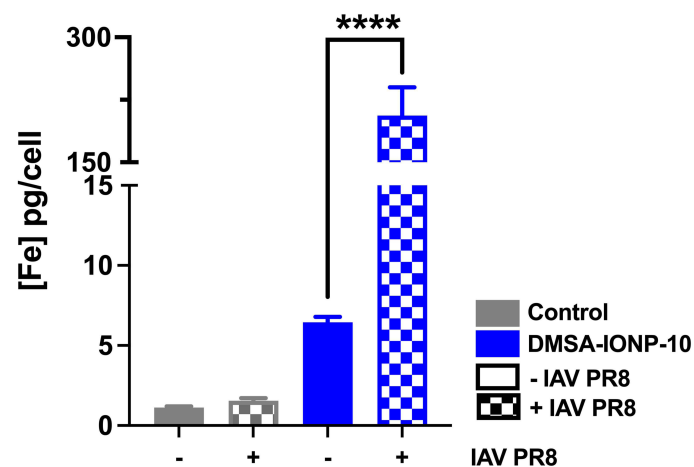
**Figure 7** Effect of DMSA-IONP-10 on the induction of oxidative stress and how oxidative stress influences the antiviral activity of DMSA-IONP-10.

**Notes:** (A) ROS generation observed by DHR fluorescence and quantitative image analysis of DHR fluorescence intensity using Image J software: Control (-) untreated A549 cells; and control (+) A549 cells incubated with 1mM H<sub>2</sub>O<sub>2</sub>. Images were taken with a 63X oil objective under a 3X zoom and the DHR fluorescence of at least 200 cells/condition is shown. (B) Quantification of gene expression by RT-qPCR (mRNA levels) in A549 cells after treatment with DMSA-IONP-10. The expression following oxidative stress was compared to that in untreated cells and the data were normalized to the expression of *GAPDH*. (C) Effect of ROS on the antiviral activity of DMSA-IONP-10. Confluent Vero E6 cells were treated for 24 h with N-acetylcysteine (NAC) or left untreated as a control. The cells were then infected with IAV (MOI 3) and 1 hpi, the extracellular medium containing the virus was replaced with a suspension of DMSA-IONPs-10, with or without NAC (200 μM). The medium was collected from the cells at 48 hpi and titrated. The data are the mean ± SD (N = 3). Differences on ROS production were analyzed with one-way analysis of variance (ANOVA) with a Dunnett's multiple comparisons test, differences on antioxidant gene expression were analyzed with a t-test and differences on the effect of ROS on virus titer were analyzed with a one-way ANOVA with Tukey's multiple comparison test: \*p < 0.05, \*\*p < 0.01, \*\*\*p < 0.001, \*\*\*\*p < 0.0001.

(1.12 pg Fe/cell) than in IAV-infected control cells (1.55 pg Fe/cell). As expected, the iron concentration increased following treatment with DMSA-IONP-10 relative to the untreated control cells. Interestingly, these concentrations of iron were higher in the treated cells previously infected with IAV than in the non-infected cells, suggesting that IAV infection facilitated the uptake of the DMSA-IONP-10 (Figure 8A).

We previously reported that treating cells with DMSA-IONP-10 altered the expression of genes involved in iron metabolism or transport.<sup>19,48–50</sup> These IONPs provoked changes in genes related to iron metabolism,<sup>19</sup> augmenting 21-fold the expression of FPN1 (*SLC40A1*) that exports iron from the cell,<sup>51</sup> inducing a 3-fold increase in the expression of the HRG1 (*SLC48A1*) that accumulates in the endosomal compartments and that has been implicated in the translocation of iron to the cytosol,<sup>52</sup> and increasing 7-fold the expression of *LCN2*, which encodes the NGAL that attaches to and

### A Effect of virus infection on DMSA-IONP entry



### B Effect of IONPs on iron metabolism in infected cells

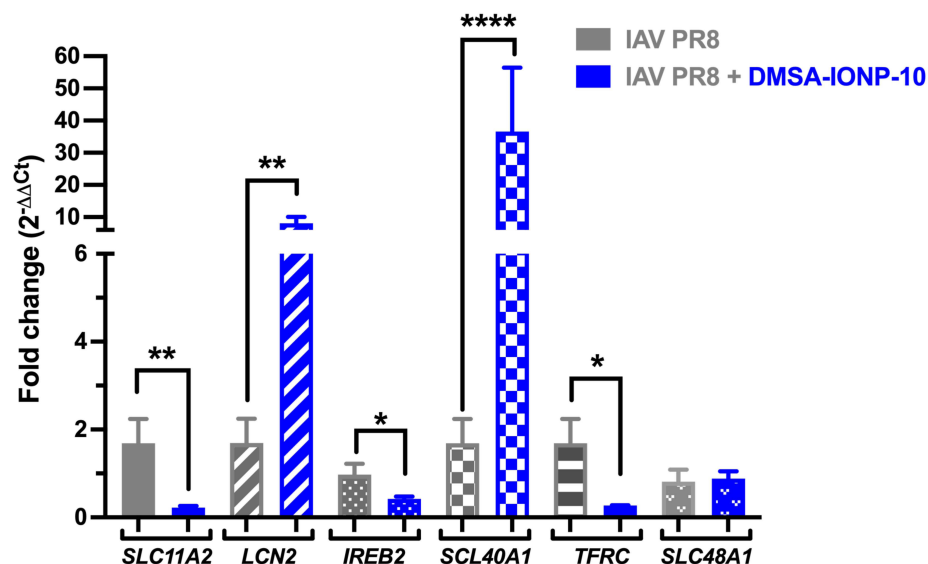


**Figure 8** Effect of DMSA-IONP-10 on iron metabolism.

**Notes:** (A and B) Vero E6 cells were infected with IAV (MOI 1) and the cells were then treated at 1 hpi with DMSA-IONP-10 (250 μg Fe/mL) for 24 h. (A) Intracellular iron was measured by ICP-OES and expressed as pg Fe/cell. (B) Total RNA was purified from the cells at 24 hpi, and the expression of *SLC11A2*, *LCN2*, *IREB2*, *SLC40A1*, *TFRC* and *SLC48A1* was analyzed by RT-qPCR, normalized to the *GAPDH* expression in each sample and represented as the fold-change relative to mock-infected cells. The data is shown as the mean ± SD (N = 3) and analyzed with a *t*-test or a two-way analysis of variance (ANOVA), and with a Tukey's multiple comparisons test: \**p* < 0.05, \*\**p* < 0.01, \*\*\**p* < 0.0001.



sequesters iron in the cytosol, thereby reducing the total cytoplasmic iron available.<sup>53</sup> By contrast, DMSA-IONP-10 did not significantly affect the expression of *TFRC*, the transferrin receptor that enables iron ions to attach to transferrin and to enter the cell,<sup>54</sup> DMT1 (*SLC11A2*) that facilitates iron entry into the cell and that also moves iron ions from the endosomal compartments to the cytosol,<sup>55</sup> or *IREB2* that encodes a transcription factor involved in iron metabolism.<sup>19,55</sup> Consequently, these IONPs appear to hijack the total free-iron in the cytoplasm and induce intense iron export from the cell, probably diminishing iron ion bioavailability.

To determine if DMSA-IONP-10 affect iron metabolism genes in the context of viral infection, control Vero E6 cells were infected with IAV (MOI 1) and treated with DMSA-IONP-10 at 1 hpi for 24 h. Viral infection mildly enhanced (around 2-fold) the expression of *LCN2*, *SLC40A1* and *TFRC* (Figure 8B), in accordance with the ICP-OES data showing slightly more intracellular iron in IAV-infected cells relative to the mock-infected cells (Figure 8A). After viral infection, treating cells with DMSA-IONP-10 dampened the expression of *SLC11A2* by 7.7-fold relative to the mock-infected cells and it increased the expression of *LCN2* by 8.1-fold (Figure 8B), probably decreasing the amount of iron available in the cytoplasm.<sup>53,56</sup> Similarly, the treatment of IAV-infected cells with DMSA-IONP-10 increased the expression of *SLC40A1* by 36.6-fold (Figure 8B), while the expression of *TFRC* decreased by 6.3-fold (Figure 8B), again probably reducing the available iron in the cell.<sup>56</sup>

## Discussion

Recently we tested the antiviral activity against SARS-CoV-2 of IONPs and we found that magnetic IONPs produced by thermal decomposition in organic medium, with a core diameter of 10 nm and coated with DMSA (DMSA-IONP-10), were the IONPs with the strongest antiviral activity.<sup>19</sup> In addition, in an earlier study, our group also studied the toxicity and biotransformation of DMSA-IONP-10 in mice, showing that after i.v. injection, DMSA-IONP-10 nanoparticles accumulated in spleen, liver and lung tissues where they undergo a process of biodegradation. Some signs of toxicity were observed post-administration, but these were transient and did not compromise mouse survival.<sup>32</sup> Because the excellent antiviral activity in vitro of DMSA-IONP-10 and their biocompatibility in mice, we decided to test in vivo the antiviral activity of DMSA-IONP-10 in mouse models of infection with SARS-CoV-2. In this study we also tested the antiviral activity of DMSA-IONP-10 against IVA in vitro and in vivo.

Although some manuscripts describe the antiviral effect of IONPs in vitro, as far as we know, none of them have shown the antiviral effect of the IONPs by treating mice with the nanoparticles after the IAV and SARS-CoV-2 infections, mimicking a therapeutic scenario, as performed in this work. Therefore, in this aspect, this work presents novelty. In previous works, IAVs were incubated with IONPs, showing that the treatment of IAVs with the IONPs dampens the infectivity of the viruses. To this end, tissue culture cells<sup>57</sup> and mice<sup>21</sup> were infected with the IAVs previously incubated with IONPs, showing the reduced infectivity of the treated IAVs.<sup>21,57</sup> However, these experiments in these other manuscripts are different from our experiments,<sup>21</sup> since we first infect the mice, and then, we treat the mice with the IONPs. Furthermore, other manuscripts describe the potential use of IONPs as SARS-CoV-2 antivirals<sup>58,59</sup> and in one of them<sup>58</sup> the authors perform docking experiments revealing that IONPs could interact efficiently with the SARS-CoV-2 receptor binding domain in the spike protein, likely preventing virus entry.<sup>58</sup> However, none of them<sup>58,59</sup> provide any experimental evidence for the antiviral effect of the IONPs. In addition, in this work we used two different viruses, very different from a genetic and molecular point of view, and the IONPs antiviral activity, even in mice, is observed for both of them, strongly suggesting that these IONPs could be further developed for the treatment of other viruses, and even for the treatment of new emerging viruses.

Related to other metal NPs, a study describes the anti-IAV effect of silver NPs (AgNPs) after administering the AgNPs intranasally to mice.<sup>23</sup> In addition, there is one very recent paper showing the antiviral effect of silver nanoparticles (AgNPs) against IAV in mice.<sup>60</sup> However, in that study the AgNPs are administered directly into the lungs prior to infection,<sup>60</sup> and not after the infection, as in our study. Selenium NPs (SeNPs) display antiviral activity against IAV, and this antiviral activity of SeNPs can be increased by coating the SeNPs with beta-thujaplicin (TP), an antimicrobial pentatrieneone (SeNPs-TP). Interestingly, in this case, the intranasal treatment of mice with the SeNPs-TP after IAV infection prevents the lung pathology induced after the infection and viral replication and increases mice

survival after the infection.<sup>31</sup> However, the molecular mechanisms mediating the in vivo antiviral activity of AgNPs and SeNPs are likely different from those of IONPs.

We acknowledge that reductions of 3 to 4-fold in virus titers in mice lungs after the treatment with the IONPs is a limited reduction and could compromise the development of these IONPs as treatments against viral infections. However, in the future we propose to improve the administration route, such as a higher proportion of IONPs reach the lungs, as well as to functionalize the IONPs with different molecules directing the IONPs to the respiratory tract. Furthermore, further studies leaving the infected mice for more than 4 days will be performed in order to get a better insight of the antiviral effect of these IONPs. Paxlovid, a combination of an orally available M<sup>pro</sup> inhibitor termed nirmatrelvir (or PF-07321332) and ritonavir,<sup>61,62</sup> has been approved as an oral treatment against COVID-19. Despite its effectiveness at reducing viral titers and the risk of progressing to severe COVID-19 in humans,<sup>63</sup> the treatment of transgenic mice expressing human ACE2 with nirmatrelvir, starting at 6 h after the infection only led to a 1.5-fold reduction in lung SARS-CoV-2 titers at 5 dpi, compared to the non-treated mice,<sup>64</sup> a reduction of viral titers even weaker to the one we observe in this study with the IONPs. In addition, in contrast to the antiviral effect of the IONPs, which is directed to cellular components, the M<sup>pro</sup> inhibitor termed nirmatrelvir (the active compound of Paxlovid) is targeted to the SARS-CoV-2 viral protease. Similarly, most of the antiviral agents which have been approved to combat IAV infections, target viral proteins. Therefore, the presence of resistance-conferring mutations in sequenced viral genomes raises concerns about future viral resistance to these compounds, and in this sense, antiviral treatments against cellular components, such as the IONPs treatments, may present advantages. Moreover, IONPs present beneficial effects over other metal nanoparticles such as the ability to adapt the size and shape to change functionality, a large concentration of paramagnetic ions in each particle, low toxicity, well-biodegradability, well-biocompatibility, and the option for additional functionality by attaching biocompatible molecules to the surface of the coatings.<sup>65</sup>

As DMSA-IONP-10 impaired SARS-CoV-2 replication prophylactically, these data suggest that the prophylactic antiviral effect of these IONPs may arise through their modulation of iron metabolism in the cells,<sup>19</sup> an effect that would be specific to the presence of Fe in the chemical composition of the IONPs. Indeed, it is accepted that viruses generally require enhanced cell metabolism to prosper, as well as high levels of iron to replicate.<sup>66</sup> The results of this study showed that IAV-infected cells increased iron content compared to uninfected cells and that IAV infection also facilitated the uptake of DMSA-IONP-10. In addition, the increase in iron content in IAV-infected cells treated with DMSA-IONP-10 induced changes in genes related to iron metabolism. Part of the biological effect of IONPs is due to the release of iron (II) (Fe<sup>2+</sup>) from endosomes/lysosomes into the cytosol as a result of IONP degradation. The alteration of the intracellular iron pool triggers changes in the iron regulatory machinery to balance iron uptake and export and to tightly regulate the intracellular concentration of the iron pool. Labile iron could either be destined for transport to organelles such as mitochondria, stored, or exported.<sup>67</sup> Therefore, the increase in total iron levels in IAV-infected cells treated with DMSA-IONP-10 triggered the downregulation of iron import-related genes such as TFRC and SLC11A2 to limit new iron import, but also triggered the overexpression of the iron export gene SLC40A1 by 36.6-fold and the iron sequestering gene LCN2 by 8.1-fold. Thus, the increase in the latter two genes would suggest that although total iron increases, cells tend to export and sequester the free iron ions, thereby increasing the amount of bound iron but decreasing the amount of free iron. Together, the data of this study suggested that the free iron available in the cells decrease in IAV-infected cells treated with DMSA-IONP-10 relative to the infected untreated cells, which could to some extent explain how the viral infection may be inhibited by these IONPs. Indeed, increasing the iron available in human bronchial epithelial cells increases IAV titers from 24 hpi.<sup>68</sup> Similarly, iron overload is an important mechanism contributing to the pathogenesis of other viral infections, such as those provoked by hepatitis B, hepatitis C, HIV-1 and human cytomegalovirus.<sup>69–73</sup> Reducing the iron available in infected cells can inhibit the growth of these viruses and the development of the diseases induced by these viruses.<sup>74,75</sup> Furthermore, IAV entry is diminished in the absence of TFRC<sup>76</sup> and consequently, pharmacological targeting of TFRC can efficiently interfere with IAV replication,<sup>76</sup> such that the decrease in TFRC in IAV-infected cells treated with DMSA-IONP-10 could be in part responsible for the lower viral titers observed in these cells. Moreover, the direct manipulation of iron metabolism by viruses and the ensuing imbalance in iron homeostasis caused by viruses represents a critical aspect of viral pathogenesis (eg SARS-CoV-2 pathogenesis).<sup>77</sup> Lower serum iron and high serum ferritin levels are correlated with disease severity in IAV-H7N9-infected patients and can predict fatal

outcomes.<sup>78</sup> Moreover, a preliminary study showed that the infection of cells with a swine influenza virus inhibited the activation of the GPX4 axis, a signaling pathway that protects against iron-dependent ferroptotic cell death. Hence, there appears to be an association between IAV and ferroptosis that results in lipid peroxidation and GSH depletion.<sup>79</sup>

As DMSA-IONP-10 induced oxidative stress in cell lines, and the treatment together with NAC reduced DMSA-IONP-10 intrinsic ability to reduce viral titers, this data suggested a ROS-dependent antiviral activity of DMSA-IONP-10. Previous studies with IONPs, AgNPs and SeNPs also demonstrated a ROS-related antiviral activity of these NPs,<sup>21,25,29</sup> although the molecular mechanism of ROS production varies, thus the biological outcomes could differ. IONPs basically depend on Fenton-like reactions to produce hydroxyl radicals (OH)<sup>80</sup> by the reaction with hydrogen peroxide, whereas AgNPs and SeNPs induce the production of superoxide radicals (O<sup>2-</sup>). The pro-oxidant mechanism of AgNPs depends on the release of Ag<sup>+</sup> ions that lead to the production of O<sup>2-</sup> via the reaction with oxygen<sup>81</sup> and the pro-oxidant mechanism of SeNPs depends on the reduction by Trx/TrxR/GSH/GR/GRx (thioredoxins/ thioredoxin reductases/ glutathione/ glucocorticoid receptor/ glutaredoxins) pathway to form selenide anion (Se<sup>-</sup>) which further forms O<sup>2-</sup>.<sup>82</sup> The different nature of the ROS produced, OH or O<sup>2-</sup>, among the different NPs can impact differently on the oxidative capacity of the NPs, as both ROS have different redox potentials, understood as the capacity to exchange electrons. The radical OH is the most powerful oxidant among the ROS with a potential of 2.34V, whereas O<sup>2-</sup> has a potential of 0.93V,<sup>83</sup> therefore the oxidative damage could be higher for IONPs than for AgNPs or SeNPs. In addition, we previously determined the oxidative capacity of different sizes and coatings of IONPs and DMSA-IONP-10 was shown to be the most oxidative IONP, causing a ten-fold change in ROS production in VeroE6 cells.<sup>19</sup>

## Conclusions

The antiviral potential of DMSA-IONP-10 to treat and/or prevent IAV infection was assessed, concluding that DMSA-IONP-10 have a prophylactic and therapeutic effect against IAV infection in Vero E6 and A549 cells at doses that are not cytotoxic. Moreover, the DMSA-IONP-10 also display therapeutic antiviral effects against SARS-CoV-2 and IAV in mice. The decrease in viral titers suggests that DMSA-IONP-10 could interfere with viral load and hence, viral pathogenesis. DMSA-IONP-10 can induce significant oxidative stress in A549 cells, activating different antioxidant effects. The weaker IAV antiviral activity in the presence of NAC, a ROS scavenger, suggests that the induction of oxidative stress in the cells by DMSA-IONP-10 was at least partially responsible for their antiviral effects. Treating cells with DMSA-IONP-10 also affects the expression of host genes involved in iron metabolism and transport. Modifying the expression of genes involved in iron metabolism and transport in IAV-infected cells may decrease the iron available in the cytoplasm, which may be at least partially responsible for the antiviral activity of DMSA-IONP-10. Together these results suggest that DMSA-IONP-10 may be used therapeutically as a treatment against SARS-CoV-2 and IAV infections. Future research should focus on optimizing their formulation and exploring their immune system interactions to enhance clinical efficacy and safety.

## Data Sharing Statement

All the data generated or analyzed during this study are included in this published article and its Additional files.

## Ethics Approval and Consent to Participate

All the protocols involving experimentation on mice were approved by the Consejo Superior de Investigaciones Científicas (CSIC) ethics committee for animal experimentation and by the Division of Animal Protection of the regional government of Madrid, and they followed National and European Union legislation on animal experimentation (PROEX125.7/21 for IAV infections and PROEX49.6/23 for SARS-CoV-2 infections; and the EC Directive 2010/63/EU). The research carried out did not involve any experimentation on human subjects.

## Acknowledgments

The authors acknowledge the assistance of the Transmission electron microscopy and Advanced light microscopy services, the Animal facility, and the Biosafety department at the National Centre for Biotechnology (CNB-CSIC). The authors also acknowledge the Animal facility at the Center for Animal Health Research (CISA-INIA-CSIC). We also

wish to acknowledge the assistance of the chemical and thermal analysis service of the Institute of Materials Science of Madrid (ICMM-CSIC). The authors are also grateful to M. Sefton for author editing of the manuscript.

## Author Contributions

All authors made a significant contribution to the work reported, whether that is in the conception, study design, execution, acquisition of data, analysis and interpretation, or in all these areas; took part in drafting, revising or critically reviewing the article; gave final approval of the version to be published; have agreed on the journal to which the article has been submitted; and agree to be accountable for all aspects of the work.

## Funding

This work was supported by the Spanish National Research Council Interdisciplinary Thematic Platform (PTI) Global Health (PTI Salud Global) [CSIC-COV19-012/012202020E154]; the European Commission-NextGenerationEU (Regulation EU2020/2094) through CSIC's Global Health Platform (PTI Salud Global) [SGL2103021]; the MCIN/AEI/10.13039/501100011033 and the "European Union NextGenerationEU/PRTR" [PDC2021-120759-I00]; the MCIN/AEI/10.13039/501100011033 [PID2020-112685RB-I00 and PID2020-113480RB-I00]; the MCIU/AEI/10.13039/501100011033 and FEDER, EU [PID2023-146212OB-I00]; the "Atracción de Talento Investigador" programme funded by the "Comunidad de Madrid" [2017-T1/BMD-515]; the Marie Skłodowska-Curie Actions programme (EU) [101007629-NESTOR-H2020-MSCARISE-2020]. In relation to the work presented here, Y. Portilla was first a predoctoral FPU scholar [FPU15/06170] funded by MCIN/AEI/10.13039/501100011033 and by "ESF Investing in your future", then a predoctoral scholar funded by CSIC-COV19-012/012202020E154, and finally, a postdoctoral scholar funded by the European Commission-NextGenerationEU (Regulation EU2020/2094) through the CSIC's Global Health Platform (PTI Salud Global) [SGL2103021]. P. Vázquez-Utrilla was a predoctoral scholar funded by the European Commission-NextGenerationEU (Regulation EU2020/2094) through the CSIC's Global Health Platform (PTI Salud Global) [SGL2103012]. V. Mulens-Arias was a postdoctoral scholar working under a Juan de La Cierva-Incorporación Contract [IJCI-2017-31447] funded by MCIN/AEI/10.13039/501100011033. N. Daviu was a predoctoral scholar [FPU18/04828] funded by MCIN/AEI/10.13039/501100011033 and by "ESF Investing in your future". The project that gave rise to these results received the support of a fellowship from "la Caixa" Foundation (ID 100010434). The fellowship code is LCF/BQ/DR22/11950020 (to D. López-García). This research work was performed in the framework of the Nanomedicine CSIC HUB (ref: 202180E048).

## Disclosure

The authors report no conflicts of interest in this work.

## References

1. COVID-19 epidemiological update – 6 November 2024. Available from: <https://www.who.int/publications/m/item/covid-19-epidemiological-update-edition-173>. Accessed November 11, 2024.
2. Javanian M, Barary M, Ghebrehewet S, Koppolu V, Vasigala V, Ebrahimpour S. A brief review of influenza virus infection. *J Med Virol*. 2021;93(8):4638–4646. doi:10.1002/jmv.26990
3. Shi J, Zeng X, Cui P, Yan C, Chen H. Alarming situation of emerging H5 and H7 avian influenza and effective control strategies. *Emerg Microbes Infect*. 2023;12(1):2155072. doi:10.1080/22221751.2022.2155072
4. Uyeki TM, Peiris M. Novel avian influenza A virus infections of humans. *Infect Dis Clin North Am*. 2019;33(4):907–932. doi:10.1016/j.idc.2019.07.003
5. Bailey ES, Choi JY, Fieldhouse JK, et al. The continual threat of influenza virus infections at the human-animal interface: what is new from a one health perspective? *Evol Med Public Health*. 2018;2018(1):192–198. doi:10.1093/emph/eoy013
6. Chen PY, Wang JT, Chang SC. Antiviral therapy of coronavirus disease 2019 (COVID-19). *J Formos Med Assoc*. 2023;123(Suppl 1):S47–S54. doi:10.1016/j.jfma.2023.08.029
7. Dave B, Shah KC, Chorawala MR, et al. Molnupiravir: an antiviral drug against COVID-19. *Arch Virol*. 2023;168(10):252. doi:10.1007/s00705-023-05881-9
8. Fernando K, Menon S, Jansen K, et al. Achieving end-to-end success in the clinic: pfizer's learnings on R&D productivity. *Drug Discov Today*. 2022;27(3):697–704. doi:10.1016/j.drudis.2021.12.010
9. Focosi D, McConnell S, Casadevall A, Cappello E, Valdiserra G, Tuccori M. Monoclonal antibody therapies against SARS-CoV-2. *Lancet Infect Dis*. 2022;22(11):e311–e326. doi:10.1016/S1473-3099(22)00311-5



10. Jahanshahlu L, Rezaei N. Monoclonal antibody as a potential anti-COVID-19. *Biomed Pharmacother.* 2020;129:110337. doi:10.1016/j.biopha.2020.110337
11. Balannik V, Wang J, Ohigashi Y, et al. Design and pharmacological characterization of inhibitors of amantadine-resistant mutants of the M2 ion channel of influenza A virus. *Biochemistry.* 2009;48(50):11872–11882. doi:10.1021/bi9014488
12. Scott C, Kankanala J, Foster TL, et al. Site-directed M2 proton channel inhibitors enable synergistic combination therapy for rimantadine-resistant pandemic influenza. *PLoS Pathog.* 2020;16(8):e1008716. doi:10.1371/journal.ppat.1008716
13. Świerczyńska M, Mirowska-Guzel DM, Pindelska E. Antiviral drugs in influenza. *Int J Environ Res Public Health.* 2022;19(5):3018. doi:10.3390/ijerph19053018
14. Moscona A. Neuraminidase inhibitors for influenza. *N Engl J Med.* 2005;353(13):1363–1373. doi:10.1056/NEJMra050740
15. Pradhan D, Biswasroy P, Goyal A, Ghosh G, Rath G. Recent advancement in nanotechnology-based drug delivery system against viral infections. *AAPS Pharm Sci Tech.* 2021;22(1):47. doi:10.1208/s12249-020-01908-5
16. Yadavalli T, Shukla D. Role of metal and metal oxide nanoparticles as diagnostic and therapeutic tools for highly prevalent viral infections. *Nanomedicine.* 2017;13(1):219–230. doi:10.1016/j.nano.2016.08.016
17. Chakravarty M, Vora A. Nanotechnology-based antiviral therapeutics. *Drug Deliv Transl Res.* 2021;11(3):748–787. doi:10.1007/s13346-020-00818-0
18. Singh CK, Sodhi KK. The emerging significance of nanomedicine-based approaches to fighting COVID-19 variants of concern: a perspective on the nanotechnology's role in COVID-19 diagnosis and treatment. *Front Nanotechnol.* 2023;4. doi:10.3389/fnano.2022.1084033
19. DeDiego ML, Portilla Y, Daviu N, et al. Iron oxide and iron oxyhydroxide nanoparticles impair SARS-CoV-2 infection of cultured cells. *J Nanobiotechnol.* 2022;20(1):352. doi:10.1186/s12951-022-01542-2
20. Kumar R, Nayak M, Sahoo GC, et al. Iron oxide nanoparticles based antiviral activity of H1N1 influenza A virus. *J Infect Chemother.* 2019;25(5):325–329. doi:10.1016/j.jiac.2018.12.006
21. Qin T, Ma R, Yin Y, et al. Catalytic inactivation of influenza virus by iron oxide nanozyme. *Theranostics.* 2019;9(23):6920–6935. doi:10.7150/thno.35826
22. xi XD, Chen Q, Pang L, long ZC. Inhibitory effects of silver nanoparticles on H1N1 influenza A virus in vitro. *J Virol Methods.* 2011;178(1–2):137–142. doi:10.1016/j.jviromet.2011.09.003
23. Xiang D, Zheng Y, Duan W, et al. Inhibition of A/Human/Hubei/3/2005 (H3N2) influenza virus infection by silver nanoparticles in vitro and in vivo. *Int J Nanomed.* 2013;8:4103–4113. doi:10.2147/IJN.S53622
24. Mori Y, Ono T, Miyahira Y, Nguyen VQ, Matsui T, Ishihara M. Antiviral activity of silver nanoparticle/chitosan composites against H1N1 influenza A virus. *Nanoscale Res Lett.* 2013;8(1):93. doi:10.1186/1556-276X-8-93
25. Li Y, Lin Z, Zhao M, et al. Silver nanoparticle based codelivery of oseltamivir to inhibit the activity of the H1N1 influenza virus through ROS-mediated signaling pathways. *ACS Appl Mater Interfaces.* 2016;8(37):24385–24393. doi:10.1021/acsami.6b06613
26. Lin Z, Li Y, Guo M, et al. The inhibition of H1N1 influenza virus-induced apoptosis by silver nanoparticles functionalized with zanamivir. *RSC Adv.* 2017;7(2):742–750. doi:10.1039/C6RA25010F
27. Lin Z, Li Y, Guo M, et al. Inhibition of H1N1 influenza virus by selenium nanoparticles loaded with zanamivir through p38 and JNK signaling pathways. *RSC Adv.* 2017;7(56):35290–35296. doi:10.1039/C7RA06477B
28. Li Y, Lin Z, Guo M, et al. Inhibitory activity of selenium nanoparticles functionalized with oseltamivir on H1N1 influenza virus. *Int J Nanomed.* 2017;12:5733–5743. doi:10.2147/IJN.S140939
29. Li Y, Lin Z, Guo M, et al. Inhibition of H1N1 influenza virus-induced apoptosis by functionalized selenium nanoparticles with amantadine through ROS-mediated AKT signaling pathways. *Int J Nanomed.* 2018;13:2005–2016. doi:10.2147/IJN.S155994
30. Lin Z, Li Y, Gong G, et al. Restriction of H1N1 influenza virus infection by selenium nanoparticles loaded with ribavirin via resisting caspase-3 apoptotic pathway. *Int J Nanomed.* 2018;13:5787–5797. doi:10.2147/IJN.S177658
31. Wang C, Chen H, Chen D, et al. The inhibition of H1N1 influenza virus-induced apoptosis by surface decoration of selenium nanoparticles with  $\beta$ -Thujaplicin through reactive oxygen species-mediated AKT and p53 signaling pathways. *ACS Omega.* 2020;5(47):30633–30642. doi:10.1021/acsomega.0c04624
32. Mejías R, Gutiérrez L, Salas G, et al. Long term biotransformation and toxicity of dimercaptosuccinic acid-coated magnetic nanoparticles support their use in biomedical applications. *J Control Release.* 2013;171(2):225–233. doi:10.1016/j.jconrel.2013.07.019
33. Roca AG, Veintemillas-Verdaguer S, Port M, Robic C, Serna CJ, Morales MP. Effect of nanoparticle and aggregate size on the relaxometric properties of MR contrast agents based on high quality magnetite nanoparticles. *J Phys Chem B.* 2009;113(19):7033–7039. doi:10.1021/jp807820s
34. Chen KY, Santos Afonso ED, Enouf V, Isel C, Naffakh N. Influenza virus polymerase subunits co-evolve to ensure proper levels of dimerization of the heterotrimer. *PLoS Pathog.* 2019;15(10):e1008034. doi:10.1371/journal.ppat.1008034
35. Livak KJ, Schmittgen TD. Analysis of relative gene expression data using real-time quantitative PCR and the 2(-Delta Delta C(T)) Method. *Methods.* 2001;25(4):402–408. doi:10.1006/meth.2001.1262
36. Wong LR, Zheng J, Wilhelmsen K, et al. Eicosanoid signalling blockade protects middle-aged mice from severe COVID-19 - PubMed. *Nature.* 2022;605(7908):146–151. doi:10.1038/s41586-022-04630-3
37. Halasi M, Wang M, Chavan TS, Gaponenko V, Hay N, Gartel AL. ROS inhibitor N-acetyl-L-cysteine antagonizes the activity of proteasome inhibitors. *Biochem J.* 2013;454(2):201–208. doi:10.1042/BJ20130282
38. Mejías R, Pérez-Yagüe S, Gutiérrez L, et al. Dimercaptosuccinic acid-coated magnetite nanoparticles for magnetically guided in vivo delivery of interferon gamma for cancer immunotherapy. *Biomaterials.* 2011;32(11):2938–2952. doi:10.1016/j.biomaterials.2011.01.008
39. Mejías R, Pérez-Yagüe S, Roca AG, et al. Liver and brain imaging through dimercaptosuccinic acid-coated iron oxide nanoparticles. *Nanomedicine.* 2010;5(3):397–408. doi:10.2217/nmm.10.15
40. Mejías R, Costo R, Roca AG, et al. Cytokine adsorption/release on uniform magnetic nanoparticles for localized drug delivery. *J Control Release.* 2008;130(2):168–174. doi:10.1016/j.jconrel.2008.05.028
41. Gutiérrez L, Mejías R, Barber DF, et al. Ac magnetic susceptibility study of in vivo nanoparticle biodistribution. *J Phys D Appl Phys.* 2011;44(25):255002. doi:10.1088/0022-3727/44/25/255002
42. Portilla Y, Mellid S, Paradelo A, et al. Iron oxide nanoparticle coatings dictate cell outcomes despite the influence of protein coronas. *ACS Appl Mater Interfaces.* 2021;13(7):7924–7944. doi:10.1021/acsami.0c20066



43. Costela-Ruiz VJ, Illescas-Montes R, Puerta-Puerta JM, Ruiz C, Melguizo-Rodríguez L. SARS-CoV-2 infection: the role of cytokines in COVID-19 disease. *Cytokine Growth Factor Rev.* 2020;54:62–75. doi:10.1016/j.cytogfr.2020.06.001
44. Rodrigues TS, Zamboni DS. Inflammasome activation by SARS-CoV-2 and its participation in COVID-19 exacerbation. *Curr Opin Immunol.* 2023;84:102387. doi:10.1016/j.coi.2023.102387
45. Ma W, Belisle SE, Mosier D, et al. 2009 pandemic H1N1 influenza virus causes disease and upregulation of genes related to inflammatory and immune responses, cell death, and lipid metabolism in pigs. *J Virol.* 2011;85(22):11626–11637. doi:10.1128/JVI.05705-11
46. Itoh Y, Shinya K, Kiso M, et al. In vitro and in vivo characterization of new swine-origin H1N1 influenza viruses. *Nature.* 2009;460(7258):1021–1025. doi:10.1038/nature08260
47. Schieber M, Chandel NS. ROS function in redox signaling and oxidative stress. *Curr Biol.* 2014;24(10):R453–462. doi:10.1016/j.cub.2014.03.034
48. Mulens-Arias V, Rojas JM, Pérez-Yagüe S, Del P MM, Barber DF. Polyethylenimine-coated SPION exhibits potential intrinsic anti-metastatic properties inhibiting migration and invasion of pancreatic tumor cells. *J Control Release.* 2015;216:78–92. doi:10.1016/j.jconrel.2015.08.009
49. Mulens-Arias V, Rojas JM, Pérez-Yagüe S, Morales MP, Barber DF. Polyethylenimine-coated SPIONs trigger macrophage activation through TLR-4 signaling and ROS production and modulate podosome dynamics. *Biomaterials.* 2015;52:494–506. doi:10.1016/j.biomaterials.2015.02.068
50. Rojas JM, Sanz-Ortega L, Mulens-Arias V, Gutiérrez L, Pérez-Yagüe S, Barber DF. Superparamagnetic iron oxide nanoparticle uptake alters M2 macrophage phenotype, iron metabolism, migration and invasion. *Nanomedicine.* 2016;12(4):1127–1138. doi:10.1016/j.nano.2015.11.020
51. Mayr R, Griffiths WJH, Hermann M, et al. Identification of mutations in SLC40A1 that affect ferroportin function and phenotype of human ferroportin iron overload. *Gastroenterology.* 2011;140(7):2056–2063. doi:10.1053/j.gastro.2011.02.064
52. Korolnek T, Hamza I. Like iron in the blood of the people: the requirement for heme trafficking in iron metabolism. *Front Pharmacol.* 2014;5:126. doi:10.3389/fphar.2014.00126
53. Xiao X, Yeoh BS, Vijay-Kumar M. Lipocalin 2: an emerging player in iron homeostasis and inflammation. *Annu Rev Nutr.* 2017;37(1):103–130. doi:10.1146/annurev-nutr-071816-064559
54. Gammella E, Buratti P, Cairo G, Recalcati S. The transferrin receptor: the cellular iron gate. *Metallomics.* 2017;9(10):1367–1375. doi:10.1039/c7mt00143f
55. Czachorowski M, Lam-Yuk-Tseung S, Cellier M, Gros P. Transmembrane topology of the mammalian Slc11a2 iron transporter. *Biochemistry.* 2009;48(35):8422–8434. doi:10.1021/bi900606y
56. Muckenthaler MU, Rivella S, Hentze MW, Galy B. A red carpet for iron metabolism. *Cell.* 2017;168(3):344–361. doi:10.1016/j.cell.2016.12.034
57. Constantino JSF, de Mesquita IDS, Moraes Segundo JDP, et al. Antiviral and nontoxic dermal iron oxide nanoparticle/biopolymer coatings for cotton fabric. *ACS Appl Nano Mater.* 2024;7(12):13991–14004. doi:10.1021/acsanm.4c00951
58. Abo-Zeid Y, Ismail NSM, McLean GR, Hamdy NM. A molecular docking study repurposes FDA approved iron oxide nanoparticles to treat and control COVID-19 infection. *Eur J Pharm Sci.* 2020;153:105465. doi:10.1016/j.ejps.2020.105465
59. Martins ES, Espindola A, Britos TN, et al. Potential Use of DMSA-containing iron oxide nanoparticles as magnetic vehicles against the COVID-19 disease. *ChemistrySelect.* 2021;6(31):7931–7935. doi:10.1002/slct.202101900
60. Martín-Faivre L, Prince L, Cornu C, et al. Pulmonary delivery of silver nanoparticles prevents influenza infection by recruiting and activating lymphoid cells. *Biomaterials.* 2025;312:122721. doi:10.1016/j.biomaterials.2024.122721
61. Owen DR, Allerton CMN, Anderson AS, et al. An oral SARS-CoV-2 Mpro inhibitor clinical candidate for the treatment of COVID-19. *Science.* 2021;374(6575):1586–1593. doi:10.1126/science.aba4784
62. Marzi M, Vakili MK, Bahmanyar M, Zarenezhad E. Paxlovid: mechanism of action, synthesis, and in silico study. *Biomed Res Int.* 2022;2022:7341493. doi:10.1155/2022/7341493
63. Hammond J, Leister-Tebbe H, Gardner A, et al. Oral nirmatrelvir for high-risk, nonhospitalized adults with Covid-19. *N Engl J Med.* 2022;386(15):1397–1408. doi:10.1056/NEJMoa2118542
64. Jeong JH, Chokkakula S, Min SC, et al. Combination therapy with nirmatrelvir and molnupiravir improves the survival of SARS-CoV-2 infected mice. *Antiviral Res.* 2022;208:105430. doi:10.1016/j.antiviral.2022.105430
65. Meng YQ, Shi YN, Zhu YP, et al. Recent trends in preparation and biomedical applications of iron oxide nanoparticles. *J Nanobiotechnol.* 2024;22(1):24. doi:10.1186/s12951-023-02235-0
66. Schmidt SM. The role of iron in viral infections. *Front Biosci.* 2020;25(4):893–911. doi:10.2741/4839
67. Mulens-Arias V, Rojas JM, Barber DF. The intrinsic biological identities of iron oxide nanoparticles and their coatings: unexplored territory for combinatorial therapies. *Nanomaterials.* 2020;10(5):837. doi:10.3390/nano10050837
68. Mayall J, Pillar A, Daly K, et al. Crucial role of iron metabolism in determining outcomes of influenza A virus infection and disease. In *10.01 - Respiratory Infections and Bronchiectasis*. European Respiratory Society; 2022:877. doi:10.1183/13993003.congress-2022.877
69. Gao YH, Wang JY, Liu PY, et al. Iron metabolism disorders in patients with hepatitis B-related liver diseases. *World J Clin Cases.* 2018;6(13):600–610. doi:10.12998/wjcc.v6.i13.600
70. Fillebeen C, Pantopoulos K. Hepatitis C virus infection causes iron deficiency in Huh7.5.1 cells. *PLoS One.* 2013;8(12):e83307. doi:10.1371/journal.pone.0083307
71. Zou DM, Sun WL. Relationship between Hepatitis C Virus Infection and Iron Overload. *Chin Med J.* 2017;130(7):866–871. doi:10.4103/0366-6999.202737
72. Traoré HN, Meyer D. The effect of iron overload on in vitro HIV-1 infection. *J Clin Virol.* 2004;31(Suppl 1):S92–98. doi:10.1016/j.jcv.2004.09.011
73. Crowe WE, Maglova LM, Ponka P, Russell JM. Human cytomegalovirus-induced host cell enlargement is iron dependent. *Am J Physiol Cell Physiol.* 2004;287(4):C1023–1030. doi:10.1152/ajpcell.00511.2003
74. Liu W, Zhang S, Nekhai S, Liu S. Depriving iron supply to the virus represents a promising adjuvant therapeutic against viral survival. *Curr Clin Microbiol Rep.* 2020;7(1):1–7. doi:10.1007/s40588-020-00140-w
75. Drakesmith H, Prentice A. Viral infection and iron metabolism. *Nat Rev Microbiol.* 2008;6(7):541–552. doi:10.1038/nrmicro1930
76. Mazel-Sanchez B, Niu C, Williams N, et al. Influenza A virus exploits transferrin receptor recycling to enter host cells. *Proc Natl Acad Sci.* 2023;120(21):e2214936120. doi:10.1073/pnas.2214936120
77. Wang Y, Huang J, Sun Y, et al. SARS-CoV-2 suppresses mRNA expression of selenoproteins associated with ferroptosis, endoplasmic reticulum stress and DNA synthesis. *Food Chem Toxicol.* 2021;153:112286. doi:10.1016/j.fct.2021.112286

78. Wang H, Xiaoxin W, Xiaoxin W, et al. Iron status is linked to disease severity after avian influenza virus H7N9 infection. *Asia Pacific J Clin Nutrition*. 2020;29(3):593–602. doi:10.6133/apjcn.202009\_29(3).0019
79. Cheng J, Tao J, Li B, Shi Y, Liu H. Swine influenza virus triggers ferroptosis in A549 cells to enhance virus replication. *Virology*. 2022;19(1):104. doi:10.1186/s12985-022-01825-y
80. Wu H, Yin JJ, Wamer WG, Zeng M, Lo YM. Reactive oxygen species-related activities of nano-iron metal and nano-iron oxides. *J Food Drug Anal*. 2014;22(1):86–94. doi:10.1016/j.jfda.2014.01.007
81. Limbach LK, Wick P, Manser P, Grass RN, Bruinink A, Stark WJ. Exposure of engineered nanoparticles to human lung epithelial cells: influence of chemical composition and catalytic activity on oxidative stress. *Environ Sci Technol*. 2007;41(11):4158–4163. doi:10.1021/es062629t
82. Khurana A, Tekula S, Saifi MA, Venkatesh P, Godugu C. Therapeutic applications of selenium nanoparticles. *Biomed Pharmacother*. 2019;111:802–812. doi:10.1016/j.biopha.2018.12.146
83. Collin F. Chemical basis of reactive oxygen species reactivity and involvement in neurodegenerative diseases. *Int J Mol Sci*. 2019;20(10):2407. doi:10.3390/ijms20102407

International Journal of Nanomedicine

Dovepress

## Publish your work in this journal

The International Journal of Nanomedicine is an international, peer-reviewed journal focusing on the application of nanotechnology in diagnostics, therapeutics, and drug delivery systems throughout the biomedical field. This journal is indexed on PubMed Central, MedLine, CAS, SciSearch®, Current Contents®/Clinical Medicine, Journal Citation Reports/Science Edition, EMBase, Scopus and the Elsevier Bibliographic databases. The manuscript management system is completely online and includes a very quick and fair peer-review system, which is all easy to use. Visit <http://www.dovepress.com/testimonials.php> to read real quotes from published authors.

Submit your manuscript here: <https://www.dovepress.com/international-journal-of-nanomedicine-journal>